



Geochemical, isotopic, and mineralogical constraints on atmospheric deposition in the hyper-arid Atacama Desert, Chile

Fan Wang^a, Greg Michalski^{a,*}, Ji-hye Seo^b, Wensheng Ge^c

^a Department of Earth, Atmospheric and Planetary Sciences, Purdue University, West Lafayette, IN 47907, USA

^b Department of Chemistry, Purdue University, West Lafayette, IN 47907, USA

^c School of Earth Sciences and Resources, China University of Geosciences, Beijing, China

Received 12 September 2013; accepted in revised form 14 March 2014; available online 26 March 2014

Abstract

Modern atmospheric deposition across the Atacama was collected by an array of dust traps that stretched from the Pacific coast to the Andean altiplano, and the material was analyzed for its geochemical, mass and isotopic composition. The coastal trap had the second-highest insoluble mineral particle and highest soluble salt deposition rates due to significant inputs from the Morro Mejillones Range and the Pacific Ocean, respectively. The Andean trap had the highest insoluble mineral particle deposition owing to transport of weathered material, but the lowest deposition rate of soluble salts due to its distance from the ocean and anthropogenic sources. The removal of oceanic material was effective by the coastal mountains, while the westward transport of the Andean material was determined to be minimal. The atmospheric deposition in the inland traps was mainly from the local entrainment of surface material, inland anthropogenic emissions, and transport of marine aerosols. The nitrate isotopes ($\delta^{15}\text{N}$ and $\Delta^{17}\text{O}$) suggested that NO_x sources and NO_3^- chemistry shifted along the west–east transect, and were greatly impacted by anthropogenic emissions with soil NO_3^- being a minor source of deposited nitrogen.

© 2014 Elsevier Ltd. All rights reserved.

1. INTRODUCTION

The influence of atmospheric deposition on soil development can be enhanced in arid environments and may be the dominant soil formation mechanism in hyper-arid regions such as the Atacama Desert. The Atacama Desert in northern Chile is one of the driest places on Earth, where the water limitation results in extremely low levels of organic matter and microorganisms in the soils, and little or no plant life across much of the desert (Erickson, 1981; Navarro-Gonzalez et al., 2003; Quinn et al., 2005). These conditions restrict normal soil formation processes such as

weathering, leaching, mass/chemical transport, and biological transformations. Massive nitrate deposits, rare iodate and perchlorate salts, and chloride, sulfate, and borate salts are ubiquitous in the Atacama (Erickson, 1981). A wide range of theories have speculated on the origins of the salt deposits, but recent stable isotope evidence has indicated that a significant portion of the Atacama's nitrate, sulfate, and perchlorate salts are photochemically produced and deposited to the soil from the atmosphere (Böhlke et al., 1997; Bao et al., 2004; Michalski et al., 2004). This suggests that net mass gains from the atmospheric deposition of dust, including water-insoluble mineral particles and associated water-soluble salts, may be the major soil development mechanism in the Atacama (Dan and Yaalon, 1982; Gerson and Amit, 1987; Quade et al., 1995; Capo and Chadwick, 1999; Ewing et al., 2006; Amit et al., 2007).

* Corresponding author. Tel.: +1 765 494 3704; fax: +1 765 496 1210.

E-mail address: gmichals@purdue.edu (G. Michalski).

Atmospheric deposition also aids in the development of desert pavements, a ubiquitous geomorphic feature in arid environments. Desert pavements are characterized by a layer of closely packed, interlocking angular or rounded pebble- and cobble-sized clasts that protect the surface from wind erosion (Cooke, 1970). Insoluble mineral particles and soluble salts deposited from the atmosphere can fill between and beneath surface rock fragments, promoting the development and uplift of the pavement (McFadden et al., 1987; Anderson et al., 2002). In addition to dense desert pavements, gypsum crusts have developed in the Atacama. These gypsum crusts could potentially allow fine dust to migrate below the crust surface, trapping atmospherically deposited material in a fashion similar to desert pavements. This desert pavement/gypsum crust theory also suggests that atmospheric deposition is a key mechanism for soil formation in arid systems. Therefore, assessing the rates at which different types of material are deposited from the atmosphere is important for understanding soil formation in arid environments in general, and in the Atacama Desert in particular (McFadden et al., 1987; Reheis and Kihl, 1995).

While it is clear that atmospheric deposition plays an essential role in the Atacama's soil formation process, there still remains uncertainties about the rates, ionic composition, and sources of salts deposited in the Atacama. Rech et al. (2003) used strontium and sulfur isotopes to indicate that the Atacama gypsum/anhydrite development is mainly impacted by marine aerosols at coastal sites and the eolian reworking of Andean salar salts at inland sites, but the deposition of other material was not investigated. Ewing et al. (2006) analyzed the atmospheric deposition collected at three sites, but focused on evaluating atmospheric element flux along a north–south rainfall gradient without quantitative constraints of the relative importance of the origins of the atmospheric deposition and their importance as a function of distance inland from the coast. Also, the effect of aerosol size and composition on dry deposition rates and the role of fogs in wet deposition in the Atacama have not been systematically discussed. The extent of surface material that is recycled and the net dust flux across the Atacama remains unknown, as is the impact of modern human activities (e.g. mining, fossil fuel burning) on atmospheric deposition. Addressing these uncertainties is important for understanding how atmosphere–soil interactions influence soil formation in hyper-arid regions such as the Atacama. This may have implications for understanding surface processes on other planets, such as Mars where soil development in the absence of water has occurred for the past 600 million years (Pike et al., 2011).

In this study, we assessed the composition, rates and potential sources of atmospheric deposition along a west–east transect in the Atacama Desert. The objective was to investigate the spatial variations in modern atmospheric deposition characteristics such as mineralogy, ionic content and accumulation rates in order to explore atmospheric deposition of material from different sources that can potentially influence soil development. Previous studies indicated that there are two categories of material in atmospheric deposition in the Atacama (Rech et al., 2003; Michalski et al., 2004; Ewing et al., 2006). The first is primary aerosols

(i.e. eolian material) consisting of marine aerosols from the adjacent Pacific Ocean, surface material (e.g. surface soil, crust, and playa salts) from local entrainment, weathered mountain material, long-range-transported dust, and direct volcanic emissions (Rech et al., 2003; Mather et al., 2004; Stuut et al., 2007). The second category is secondary aerosols such as nitrates and sulfates, produced from reactive atmospheric gases (Michalski et al., 2004; Ewing et al., 2006). We hypothesize that eolian material can be carried from different source regions by winds and deposited to a west–east transect, and the relative importance of each source is a function of its proximity to a given collector. We speculate that the distribution of secondary aerosols in the atmosphere is determined by the regional emissions of precursor gases, the residence time for converting the gases into aerosols, and the removal efficiencies of the resulting aerosols along their transport paths. In modern times, human activities are hypothesized to exert a significant enhancement in the production and deposition of secondary aerosols in the Atacama basin.

2. SAMPLING AND ANALYSIS METHODS

The physiography of the Atacama Desert consists of three major geologic units going from west to east: the Coastal Range, the Central Valley and the Andes (Figs. 1 and 2). The Coastal Range is a mountain range running north and south that abuts the Pacific Ocean, has altitudes generally less than 2000 m, and is mantled by Jurassic volcanic sequences imbedded with marine and continental conglomerates (SERNAGEOMIN, 2003). The Central Valley is a longitudinal depression typically with altitudes between 900 and 2500 m, comprising a few hundred meters thick layers of Upper Miocene–Pliocene piedmont clastic sediments (SERNAGEOMIN, 2003). The Andes consist of an altiplano about 4000 m in altitude surmounted by hundreds of volcanic peaks (~5000 m), and a succession of parallel Pre-Andes mountain ranges (i.e. the Cordillera Central in the north and the Cordillera Domeyko in the south) with intervening valleys and basins; the Andes are predominately underlain by Pliocene–Quaternary volcanic flow, tuffs, and breccia rocks (SERNAGEOMIN, 2003).

An array of ten dust traps (T1–T10) were installed along a west–east transect across the Atacama to investigate the spatial variations of atmospheric deposition in the desert (Figs. 1 and 2). The selection of the dust trap locations was based on the accessibility, absence of dirt roads or other artificially disturbed areas upwind, and inconspicuousness. The traps were mostly placed in flat, relatively open areas every 10–50 km inland from the western Pacific coast (see [Supplementary Information](#) for site pictures). The traps consisted of a single-piece Bundt cake pan (outer ring diameter: 25 cm, surface area: 477 cm²) fitted with a circular piece of 0.25-inch mesh galvanized screen on which a layer of pre-washed glass marbles were placed to mimic desert pavements (Reheis and Kihl, 1995). The traps were mounted on ~1 m high poles above the ground to eliminate most saltating particles and left exposed from 7/10/2007 to 1/1/2010 (915 days). Trap 9 was destroyed during this period and is thus excluded from this study.

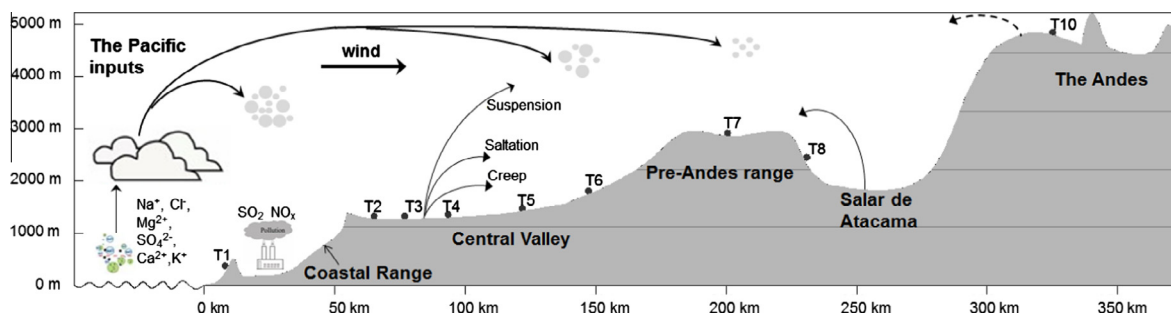


Fig. 1. Diagram showing the origins and transport of eolian material and secondary aerosols in the Atacama Desert. Seawater droplets, anthropogenic emissions and local entrainment of surface material (mainly suspension process) can be introduced to the atmosphere before they are eventually transported and deposited across the Atacama depending on their distance from the source regions as well as their compositions and sizes.

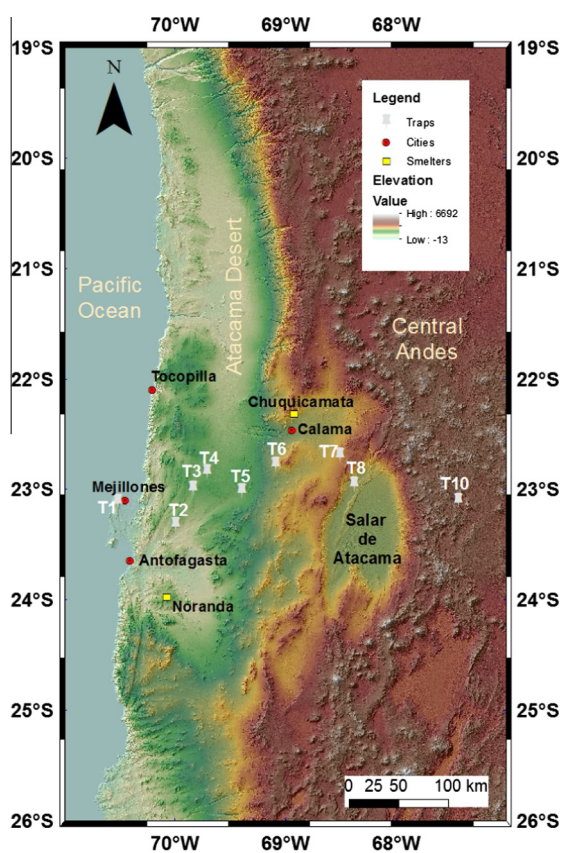


Fig. 2. Location map of the trap array along an west-east transect across the Atacama Desert, major cities and copper smelters in the Antofagasta region (T1-a barren hillslope of the Morro Mejillones; T2-a barren mountain basin with sparse desert pavements; T3-a barren hillslope with medium desert pavements; T4-a barren mountain basin with sparse desert pavements; T5-a barren alluvial fan with disturbed surface; T6-a mountain basin with dense desert pavements and dry plant roots; T7-a barren hilltop of the Cordillera de Domeyko with dense desert pavements; T8-the Atacama basin rim with salt crusts and holes; T10-a closed basin with dense desert pavements).

Atmospheric deposition collected in the traps was finally retrieved at the end of the exposure period and analyzed.

All insoluble and soluble material was removed from the traps by washing the pans, marbles and screen with deionized water into 1 L plastic bottles. The washed solutions were kept frozen and shipped to Purdue University overnight and gradually freeze-dried in the laboratory. The dried solids, considered as the bulk atmospheric deposition, were weighed to calculate deposition rates, and their mineralogical composition was determined using X-ray diffraction. The bulk dust was then washed, filtered to separate the insoluble mineral particles and soluble salts, and the filtrate was measured for pH (Fisher Science). The insoluble mineral particles were air-dried in evaporating dishes and reweighed to measure the soluble salt mass. Two 3 mL aliquots of the filtrate containing soluble salts for each sample were used to analyze cations (Ca^{2+} , K^{+} , Mg^{2+} and Na^{+}) by inductively coupled plasma-optical emission spectroscopy (ICP-OES Thermo Scientific iCAP 6500), ammonium NH_4^{+} by an automated discrete analyzer (Seal Analytical AQ2), and anions (Cl^{-} , NO_3^{-} and SO_4^{2-}) by ion chromatography (Dionex DX-500). A blank control sample was prepared by using Millipore water to rinse a new trap without dust collection, and the rinse solution went through all the processes and each analysis as for the real sample. No targeted ions have been detected in the blank control. The measurement uncertainties for different ion concentrations in this study were typically <5% based on replicate analysis of standards and calibrations. Finally, another split was withdrawn from the filtrate and $\delta^{15}\text{N}$ and $\Delta^{17}\text{O}$ values of nitrate were analyzed using a bacterial reduction, gold redox method (Kaiser et al., 2007; Riha, 2013) by Delta V Plus isotope ratio mass spectrometry (IRMS) at the Purdue Stable Isotope facility. The isotopic results were normalized to multiple laboratory working standards that were previously calibrated to international standards USGS32, USGS34 and USGS35. The precisions for $\delta^{15}\text{N}$ and $\Delta^{17}\text{O}$ values were $\pm 0.4\text{‰}$ and $\pm 0.3\text{‰}$, respectively, based on replicate analysis of the working standards and calibrations.

Fog, lake water, and snow samples were also collected and analyzed. A single fog sample was collected overnight (December 2011) at Salar de Grande (21.20°S, 70.01°W, elevation: 847 m) using a 2 m × 2 m polyethylene sheet (termed as “Grande fog” for later discussion). This location

is 8 km away from the ocean, ~230 km north of our T1 site. Lake water was collected from the Salar de Tara (23.10°S, 67.43°W, 4260 m, 1.5 km south of the T10 site, termed as “Tara lake water” for later discussion) in January of 2010, while one sample was collected from a remnant snow drift in the Salar de Tara (9 km northwest of the T10 site, termed as “Tara snow” for later discussion) in July of 2007. These samples were analyzed for cation and anion concentrations by ICP-OES and ion chromatography, respectively.

3. RESULTS

3.1. General characterization of dust deposition

The deposition rate and composition of atmospheric dust varied greatly from the coast to the Andean site (Fig. 3). The bulk dust deposition rates were highest at the Andean site T10 (35.1 g m⁻² yr⁻¹) and at the coastal site T1 (16.2 g m⁻² yr⁻¹), while the lowest was at T7 site (5.0 g m⁻² yr⁻¹), and was relatively consistent at T2–T6 and T8 sites (6.0–9.7 g m⁻² yr⁻¹). Similarly, the highest insoluble mineral particle deposition rates occurred at T10 and T1 sites, 32.6 and 12.3 g m⁻² yr⁻¹, respectively, and the T7 site had the lowest insoluble mineral deposition rate of 3.2 g m⁻² yr⁻¹. The deposition rate of soluble material (*i.e.* soluble salts and other soluble material) significantly decreased from 4.0 g m⁻² yr⁻¹ at T1 site to 2.5 g m⁻² yr⁻¹ at T2 site ~65 km inland, and stayed relatively consistent from T2–T10 (2.7 ± 0.3 g m⁻² yr⁻¹). For all traps, the soluble salts accounted for 1.4–16.6% of the bulk dust and 19–58% of the total soluble material (Fig. 3).

3.2. Mineralogical and geochemical compositions

The major mineral (>5% by mass) assemblage in atmospheric bulk deposition for T1–10 sites was anorthite–quartz–albite–gypsum (Table 1). In general, the X-ray diffraction patterns of the traps were similar but those at

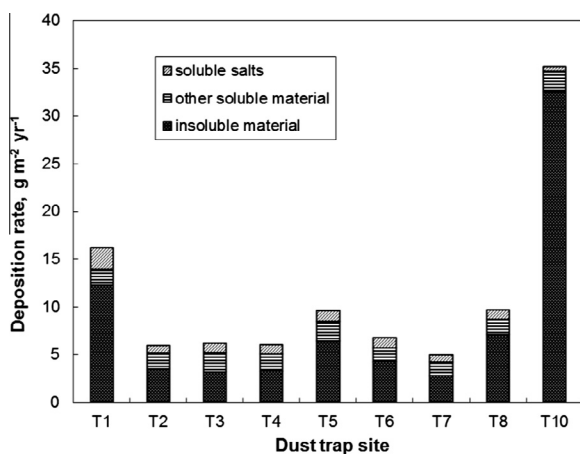


Fig. 3. The deposition rates and general composition of atmospheric deposition.

Table 1

Major mineralogy of bulk atmospheric deposition.

Sampling site	XRD results
T1	An, Qz, Ab, H, Gp
T2	An, Gp, Ab, Qz
T3	An, Gp, Qz, Ab
T4	Gp, An, Qz, Ab
T5	An, Gp, Qz, Ab
T6	An, Gp, Qz, Ab
T7	An, Gp, Qz, Ab
T8	An, Gp, Qz, Ab
T10	An, Qz, Ab

Qz: quartz (SiO₂), Ab: albite (NaAlSi₃O₈), An: anorthite (CaAl₂Si₂O₈), Gp: gypsum (CaSO₄), H: Halite (NaCl) (listed from highest to lowest amount no less than 5%).

T2–T8 sites were slightly different from those at T1 and T10 sites. For example, T1 site has a significant amount of halite, while T10 site is mainly composed of anorthite with minor amounts of albite (<5%).

Ion analysis of the soluble salts showed that all these sites were rich in Cl⁻, NO₃⁻, SO₄²⁻, Na⁺, and Ca²⁺, which totaled over 90% of the dissolvable salt mass, with small amounts of NH₄⁺, Mg²⁺ and K⁺ cations also being present (Table 2). T1 site had the highest or second-highest deposition rates of those five major ions among all sites. There was a sharp decrease in Na⁺, Cl⁻ or SO₄²⁻ amount going from T1 to T2 site, where the soluble ion deposition rates were relatively consistent from T2–T8 sites. The lowest deposition rates of the major ions occurred at the Andean site (T10). The molar ratio of Na⁺/(NO₃⁻ + Cl⁻) was approximately 1 (<10% deviations) at all sites except at T1, T6 and T10, while the Ca²⁺/SO₄²⁻ molar ratios were close to 1 at T2–T8 sites. There were relatively low NH₄⁺ deposition rates at all sites, but the highest were at T10 (0.19 mmol m⁻² yr⁻¹) and T1 (0.18 mmol m⁻² yr⁻¹) sites with the lowest at T2–T8 sites ranging from 0.02 to 0.10 mmol m⁻² yr⁻¹. Mg²⁺ deposition continuously decreased from the rate of 1.25 mmol m⁻² yr⁻¹ at T1 site to 0.31 mmol m⁻² yr⁻¹ at T10 site. A similar sharp decrease was observed for K⁺ deposition rate from T1 coastal site to T2 inland site, but it fluctuated at T2–T10 sites. The ionic charge was almost balanced (<15% deviations) at all sites other than T10.

3.3. Variations in isotopic composition of nitrate

The isotopic composition of the nitrate salt (NO₃⁻) also showed spatial differences from the coast to the Andes (Fig. 4). The NO₃⁻ δ¹⁵N ranged from +1.5‰ to +10.6‰, and while the NO₃⁻ δ¹⁵N value generally decreased from the coast (+8.5‰) to the inland sites with the lowest value at T8 site, an abrupt increase to the highest value was observed at T10 site. The NO₃⁻ Δ¹⁷O values were in a relatively narrow range of 24.0–27.8‰ with the highest value occurring at T1 site and the lowest value at T10 site. Sample replicates had mean standard deviations of 0.5‰ for δ¹⁵N and 0.5‰ for Δ¹⁷O (*n* = 3 for each sample set).

Table 2
Deposition rates of the soluble ions ($\text{mmol m}^{-2} \text{yr}^{-1}$) and the molar ratios.

Sampling site	NH_4^+	Ca^{2+}	K^+	Mg^{2+}	Na^+	Cl^-	NO_3^-	SO_4^{2-}	$\text{Ca}^{2+}/\text{SO}_4^{2-}$	$\text{Na}^+(\text{Cl}^- + \text{NO}_3^-)$	Positive/negative charge	pH
<i>Coastal site</i>												
T1	0.18	4.10	0.93	1.25	23.90	11.05	3.47	9.53	0.43	1.65	1.06	7.03
<i>Andean site</i>												
T10	0.19	1.55	0.18	0.31	2.20	2.86	0.54	2.37	0.65	0.65	0.77	5.04
<i>Inland sites</i>												
T2	0.05	3.54	0.22	0.79	4.13	1.39	2.88	3.69	0.96	0.97	1.12	4.71
T3	0.04	3.19	0.35	0.75	5.24	0.96	4.62	4.01	0.79	0.94	0.99	6.03
T4	0.06	3.93	0.53	0.85	4.86	1.29	3.54	4.55	0.86	1.01	1.08	4.38
T5	0.02	4.41	0.26	0.70	6.77	1.73	4.83	4.23	1.04	1.03	1.15	6.74
T6	0.10	3.98	0.39	0.66	5.75	0.85	3.70	4.86	0.82	1.26	1.09	6.58
T7	0.03	2.89	0.16	0.37	3.48	1.11	2.74	3.51	0.82	0.91	0.94	4.64
T8	0.06	4.04	0.23	0.43	5.49	3.91	2.00	3.69	1.09	0.93	1.11	5.33
<i>Previous study</i>												
Yungay ^a	0.16	6	n.d.	n.d.	20	4	17	19	0.32	0.95	0.55	n.d.

^a From Ewing et al. (2006) except the NH_4^+ data that is from Ewing et al. (2007).

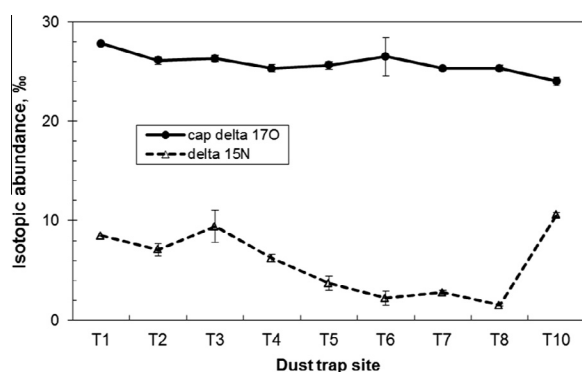


Fig. 4. The isotopic composition of trap NO_3^- .

4. DISCUSSION

The mass, mineralogical, ionic, and isotopic composition of atmospheric dust deposited along the Atacama transect from the coast to the Andes can provide insight to the characteristics of atmospheric deposition at a detailed scale and allow us to investigate possible shifts in sources of atmospheric deposition along the Atacama transect. Therefore, we will individually discuss the T1 site, the T10 site and T2–T8 sites in order to investigate the influence of oceanic inputs, Andean inputs, local entrainment of surface material, and anthropogenic emissions on the deposition of atmospheric compounds to the Atacama's surface.

4.1. The influence of marine aerosols at the coastal site T1

T1 site had the second-largest bulk dust deposition rate ($16.2 \text{ g m}^{-2} \text{ yr}^{-1}$) among the nine sites, which could be mainly accounted for by the high deposition rate of insoluble mineral particles ($12.3 \text{ g m}^{-2} \text{ yr}^{-1}$). This may have been due to T1 being located on a western hillslope of the Morro

Mejillones and the influence of weathering of silicate material and a significant down-slope dust flux. The area near T1 site may also have been subject to dust from some small surface mining operations during the collection period. The major mineral assemblage of the Morro Mejillones surface soil was anorthite–quartz–albite, similar to that of the atmospheric bulk deposition. Therefore, weathering material from the Morro Mejillones Range was a significant source of insoluble mineral particles deposited at the T1 site. The average ionic composition in the surface soil (0–10 cm) in the Morro Mejillones was: Ca^{2+} $0.006 \text{ mmol g}^{-1}$, K^+ $0.006 \text{ mmol g}^{-1}$, Mg^{2+} $0.004 \text{ mmol g}^{-1}$, Na^+ 0.05 mmol g^{-1} , Cl^- 0.08 mmol g^{-1} , NO_3^- $0.002 \text{ mmol g}^{-1}$ and SO_4^{2-} 0.01 mmol g^{-1} . The contribution of salts from the entrainment of surface soil material into our T1 trap would then be the multiplication of soil ion concentration by the insoluble dust deposition rate ($12.3 \text{ g m}^{-2} \text{ yr}^{-1}$). The fractions of the soil ions relative to the corresponding trap ions were 2%, 7%, 4%, 3%, 9%, 1% and 2% for Ca^{2+} , K^+ , Mg^{2+} , Na^+ , Cl^- , NO_3^- and SO_4^{2-} , respectively. It was evident that local soil entrainment accounts for only a small part of the ions load in the T1, except for Cl^- , and therefore, soil contribution to dust anions, other than Cl^- are neglected in the remainder of the discussion in this section. The contribution of soil Cl^- was subtracted from the observed Cl^- deposition in T1 trap yielding a non-soil Cl^- deposition rate of $10.02 \text{ mmol m}^{-2} \text{ yr}^{-1}$.

The soluble fraction of material deposited at T1 site was predominately attributed to ocean salts. Amongst all sites, T1 site had the highest soluble salt deposition rate ($4.0 \text{ g m}^{-2} \text{ yr}^{-1}$), roughly five times higher relative to the other sites. The salts were primarily composed of Na^+ and Cl^- (Table 2), the main salt components of seawater, suggesting major oceanic salt inputs at T1 site. This was not surprising given that the T1 site was located on the windward side of the Morro Mejillones range on the Mejillones Peninsula approximately 6 km away from the ocean and that sea-salt aerosols usually dominate aerosol loadings

in coastal regions (Fitzgerald, 1991; O'Dowd and de Leeuw, 2007). Further, there were no salt playas on the Mejillones Peninsula or the nearby coast (Stoertz and Ericksen, 1974) and the entrainment of material from salt playas located east of the Coastal Range to T1 site was likely trivial because of the isolation of T1 site from the mainland by the Morro Mejillones and the Coastal Range (discussed below).

Marine aerosols are comprised of primary and secondary aerosols, both of which appear to be important to ion deposition at T1 site. Primary marine aerosols are sea-salt aerosols (SSA) consisting of seawater droplets that are entrained into the atmosphere, forming particles that are mainly NaCl. The droplets originate from the bursting of air bubbles or tearing of drops off wave crests induced by the action of winds on the ocean, with the supermicron-sized ($>1\ \mu\text{m}$) particles typically dominating the aerosol volume (mass) concentration (O'Dowd and de Leeuw, 2007). These large sea-salt particles can quickly gravitationally settle (Lewis and Schwartz, 2004), explaining the high rate of NaCl deposition at T1 site. Secondary marine aerosols are mostly submicron-sized particles formed from the chemical and/or physical transformations of oceanic precursor gases in the atmosphere (O'Dowd and de Leeuw, 2007). For example, H_2SO_4 derived from dimethyl sulfide (DMS) oxidation can react on sea salts with $\text{NH}_3(\text{g})$ emitted by the ocean to form SO_4^{2-} aerosols explaining part of SO_4^{2-} in the T1 trap (Charlson et al., 1987; O'Dowd and de Leeuw, 2007). Thus, the presence of NH_4^+ in the T1 trap was also indicative of the existence of secondary marine aerosols at this site. Therefore, the T1 trap may have accumulated marine aerosols, mainly supermicron sea-salt-aerosols and submicron secondary aerosols. This hypothesis was supported by the ionic ratios of the T1 trap salts.

To investigate the contribution of SSA to the ionic load, enrichment factors (EF_{Na}) were calculated for each ion (X) relative to the seawater using $\text{EF}_{\text{Na}} = (\text{X}/\text{Na})_{\text{dust}}/(\text{X}/\text{Na})_{\text{seawater}}$, where $(\text{X}/\text{Na})_{\text{dust}}$ and $(\text{X}/\text{Na})_{\text{seawater}}$ are the ratios of the ion X to Na^+ concentration in atmospheric dust or seawater, respectively. Here, Na^+ was used as the reference trace element to calculate the enrichment factors at T1 site because Na^+ is derived predominantly from seawater, is easily determined using the ICP-OES technique, and has a high concentration in sea-salt aerosols that is insensitive to perturbation by outside sources (Keene et al., 1986). The average composition of ions in seawater was taken as: 0.546 M Cl^- , 0.468 M Na^+ , 0.0103 M Ca^{2+} , 0.0102 M K^+ , 0.0532 M Mg^{2+} ; 0.0282 M SO_4^{2-} (Millero, 1974). All of the ions showed some enrichments ($\text{EF}_{\text{Na}} > 1$), except non-soil Cl^- and Mg^{2+} , that were depleted, and Na^+ (by definition = 1.0) (Table 3). This indicated that at T1 site there was a loss of Cl^- and Mg^{2+} whilst there were sources of Ca^{2+} , K^+ , and SO_4^{2-} other than that derived from dissolved ions in seawater.

4.1.1. Evidence of aerosol Cl^- loss by acid displacement at the T1 site

The non-soil Cl^-/Na^+ of 0.42 at T1 site was much lower than the typical seawater equivalent ratio of 1.17, likely related to the reaction of NaCl aerosols with atmospheric acids. Acids such as HNO_3 and H_2SO_4 produced photochemically

Table 3

The enrichment factors (EF_{Na}) for different ions in the trap and fog samples.

Species	Coastal site		
	EF_{Na} T1	EF_{Na} El Tofo fog	EF_{Na} Grande fog
Ca^{2+}	7.8	5.2	21.7
K^+	1.8	2.1	3.7
Mg^{2+}	0.5	1.1	1.0
Na^+	1.0	1.0	1.0
Cl^-	0.4	0.9	0.9
SO_4^{2-}	6.6	7.5	6.9

in the atmosphere can displace Cl^- by liberating the more volatile acid $\text{HCl}_{(\text{g})}$ (Ayers et al., 1999; Newberg et al., 2005), resulting in the loss of Cl^- from aerosols to the air column. This is consistent with the observations of Cl^- deficits in marine aerosols, and especially, smaller aerosols are more depleted in Cl^- owing to their higher surface to volume ratios (Harkel, 1997). During our rainless collection period with typical wind speeds of $3\text{--}10\ \text{m s}^{-1}$, these Cl^- depleted aerosols could have rapidly dry deposited to the land surface (including T1 trap) with the dry deposition velocity of $1\text{--}6.5\ \text{cm s}^{-1}$ (McDonald et al., 1982). Some dry deposition of volatilized $\text{HCl}_{(\text{g})}$ may have also occurred in the trap by interacting with its surface material, but it was unlikely retained because of its high volatility and the inertness of the glass marbles. Assuming Cl^- was mainly lost by the displacement reaction with HNO_3 and H_2SO_4 , then $[\text{Cl}^-]_{\text{loss}} = 1.17 \times \text{R}[\text{Na}^+] - \text{R}[\text{Cl}^-]$, where $\text{R}[\text{X}]$ was the deposition rate for the X ion, and 1.17 was the Cl^-/Na^+ molar ratio in the seawater. This yielded a $[\text{Cl}^-]_{\text{loss}}$ of $17.94\ \text{mmol m}^{-2}\ \text{yr}^{-1}$, a 60% Cl^- deficit when referenced to Na^+ . This deficit at T1 site was comparable to the Cl^- deficits of $\sim 50\%$ in aerosols over northern Chilean coastal waters observed during the VAMOS Ocean-Cloud-Atmosphere-Land Study field campaign (Chand et al., 2010) or the 83% Cl^- deficit in bulk atmospheric deposition $\sim 120\ \text{km}$ southeast of T1 calculated based on the data reported by Ewing et al. (2006). This chloride deficit should have been equivalent to the sum of secondary NO_3^- and SO_4^{2-} acids (excluding the SO_4^{2-} from seawater).

4.1.2. SO_4^{2-} source apportionment at the T1 site

The EF_{Na} for SO_4^{2-} was 6.6 showing that sources other than seawater have contributed to the bulk of SO_4^{2-} at the T1 site. Besides its existence in seawater, SO_4^{2-} can be produced within the atmosphere mainly by oxidation of SO_2 into sulfate by OH radicals, H_2O_2 and ozone via heterogeneous and homogeneous pathways (Khoder, 2002; Seinfeld and Pandis, 2006). These sulfates are distinguished from the sea-salt sulfate and often termed as non-sea-salt (NSS) sulfate. A substantial fraction of NSS sulfates are associated with sea-salt aerosols because the high pH of sea-salt water promotes a rapid oxidation of reduced sulfur species into NSS sulfates via ozone (Sievering et al., 1990; Song and Carmichael, 2001). However, once the sea-salt aerosol alkalinity is consumed, the H_2O_2 and halogen oxidation pathways become significant (Vogt, 1996; Keene et al., 1998). The NSS sulfate amount can be calculated based on: $\text{R}[\text{NSS SO}_4^{2-}] = (\text{EF}_{\text{Na}}(\text{SO}_4^{2-}) - 1) \times \text{R}[\text{SO}_4^{2-}]/\text{EF}_{\text{Na}}(\text{SO}_4^{2-})$. This resulted in a NSS SO_4^{2-} deposition rate of

8.1 mmol m⁻² yr⁻¹, and a corresponding seawater sulfate deposition rate of 1.4 mmol m⁻² yr⁻¹. Considering one H₂SO₄ molecule could displace two NaCl molecules during the reaction 2NaCl + H₂SO₄ → Na₂SO₄ + 2HCl, assuming this NSS sulfate was previously in the form of H₂SO₄, then it could account for most of the Cl⁻ loss with a remaining Cl⁻ deficit of 1.7 mmol m⁻² yr⁻¹.

Natural sources of the NSS SO₄²⁻ at T1 site could be volcanic and oceanic reduced sulfur emissions (*i.e.* DMS) as well as the entrainment of gypsum from salt playas. Volcanic emissions can be important over long timescales that encompass volcanic activities (Andres et al., 1991), but these were absent over the timescale of our sample collection (Source: National Geophysical Data Center/World Data Service). Gypsum from several small playas (Salar de Carmen, Salar de Navidad and Salar Mar Muerto) within 150 km southeast of T1 site (east of the Coastal Range) (Stoertz and Ericksen, 1974; Rech et al., 2003) were probably transport-limited because of the mountain barriers and predominant westward air flow (see detailed discussion below) and thus was likely a trivial source of SO₄²⁻. This suggested that DMS oxidation may have accounted for a significant fraction of NSS at T1 site. The average ocean/atmosphere DMS flux was estimated to be 1.4 ± 0.1 mmol m⁻² yr⁻¹ for the coastal regions near Antofagasta (Yang et al., 2011); slightly lower than the estimated 2.1 ± 2.4 mmol m⁻² yr⁻¹ for the gyre regions in Southeastern Pacific (Marandino et al., 2009). The latter flux was observed away from the Atacama's coast in a region with relatively high wind speeds and during the Southern Hemisphere's summer months when there were higher primary productivities. Both wind-speed and primary productivity could enhance ocean-atmosphere DMS fluxes, likely explaining the higher DMS flux in the open ocean relative to the coastal region. Based on these studies, a DMS deposition flux range of 1.3–4.5 mmol m⁻² yr⁻¹ was adopted, and by assuming all DMS was converted to an equimolar amount of NSS sulfate and deposited to the surface, this estimated DMS-derived sulfate flux could account for 16–56% of NSS sulfate. The deposition of DMS-derived sulfate could be at least equal to, or as much as three times higher, than the deposition of sea-salt sulfate along the coastal Atacama.

A check of the estimated sea-salt SO₄²⁻ and NSS deposition rates can be carried out using sulfur isotope mass balance. Rech et al. (2003) measured the δ³⁴S values of surface gypsum deposits in several Atacama coastal soils, which can be considered sulfate in the absence of human impacts and surface disturbance. The two natural sources of oceanic sulfate have distinguishable δ³⁴S values: +21.1 ± 1.9‰ for seawater SO₄²⁻ and +15.6 ± 3.1‰ for DMS-derived SO₄²⁻ (Calhoun et al., 1991). The isotopic mass balance equation is therefore: δ³⁴S_{NDEP} · R_{NDEP}[SO₄²⁻] = δ³⁴S_{sw} · R_{sw}[SO₄²⁻] + δ³⁴S_{DMS} · R_{DMS}[SO₄²⁻], where the subscripts NDEP, SW, and DMS stand for natural rates (R) of atmospheric deposition, seawater input, and DMS emission, respectively, and R_{NDEP}[SO₄²⁻] = R_{sw}[SO₄²⁻] + R_{DMS}[SO₄²⁻]. Based on our delineation between seawater and DMS SO₄²⁻ fluxes and assuming these fluxes have remained constant prior to human sulfur sources in the region, the pre-anthropogenic

sulfate δ³⁴S_{NDEP} value would range from +16.9 ± 2.5‰ to +18.4 ± 2.8‰. This was close to the δ³⁴S values (+16.6‰ to +18.3‰) of soil sulfate located 4–8 km away from the coast and ~60 km south of the T1 site (Rech et al., 2003). This demonstrated that the sulfate δ³⁴S values near the coast were slightly lower than the seawater sulfate δ³⁴S, likely due to the DMS flux rather than any imprint from the Andean weathering material as indicated by Rech et al. (2003). Thus, ignoring the importance of DMS flux has likely resulted in an overestimation of the importance of Andean weathering SO₄²⁻ inputs to the Atacama (Rech et al., 2003).

Anthropogenic reduced sulfur emissions could account for the remaining NSS sulfate. Important local anthropogenic sources of sulfur include regional power plants and copper smelters (Table 4). However, there were several lines of evidence suggesting that large amounts of anthropogenic sulfur emitted were not effectively transported to or deposited at T1 site. Firstly, most of the anthropogenic sources were inland, separated from T1 site by the Morro Mejillones and Coastal Ranges. These fog-laden mountain ranges were effective barriers for boundary layer transport of soluble compounds (discussed below). Further inland, solar heating of the western slope of the Andes caused daytime upslope air flow (Andean pump) resulting in much weaker seaward air mass returns (Rutllant et al., 2013). Analysis of atmospheric transport in 2008, during our sampling, showed that the number of easterly-wind events that could potentially pollute the coastal stratocumulus cloud deck with inland anthropogenic or natural sulfur aerosols were limited to only four to eight times per year (Huneus et al., 2006; Rutllant et al., 2013). Therefore, the inland Noranda and Chuquicamata smelters were unlikely to be able to significantly impact SO₄²⁻ deposition at the T1 site. Moreover, the prevailing wind on the coast was the onshore southwesterly, which further limited possible anthropogenic SO₄²⁻ deposition from inland sites as well as minimizing the impact of sulfur emissions in the city of Tocopilla 130 km northwest. Hence, the Mejillones Peninsula and the city of Antofagasta (mainly the Edelnor power plant) that together emitted 10,970 metric tons of SO₂ per year (1.7 × 10⁸ mol yr⁻¹) (Table 4) were likely accounting for the remaining NSS sulfate. Given an average wind speed of ~5 m s⁻¹ (Muñoz, 2008) and a SO₂ lifetime of 10–12 h in power plant plumes (Ryerson et al., 1998), the SO₂ could potentially spread over a circle area with the radius of 180–216 km area. Thus, the anthropogenic SO₂ emission rate in the T1 surrounding region could account for a SO₄²⁻ deposition rate of 4.6–6.7 mmol m⁻² yr⁻¹. In conclusion, the SO₄²⁻ deposition at T1 site was comprised of 28–62% oceanic SO₄²⁻ derived from DMS (1.3–4.5 mmol m⁻² yr⁻¹) and seawater (1.4 mmol m⁻² yr⁻¹), and 38–72% anthropogenic SO₄²⁻ (3.6–6.8 mmol m⁻² yr⁻¹).

4.1.3. NO₃⁻ and NH₄⁺ sources at the T1 site

The NO₃⁻ found in the T1 trap, similar to NSS SO₄²⁻, was produced in the atmosphere by the oxidation of nitrogen (N) compounds and may have accounted for the remainder of the chloride deficit. NO₃⁻ was deposited at a rate of 3.47 mmol m⁻² yr⁻¹, but was from secondary, not

Table 4
Major regional anthropogenic emissions.

Sources	Emissions, metric tons per year	
	NO _x	SO ₂
<i>Mejillones Peninsula</i>		
Edelnor power plant (341 MW) ^a	7128	10,951
On-road automobiles ^b	42	0.5
<i>Antofagasta city</i>		
On-road automobiles ^b	1485	18
Port activities ^c	5772	
<i>Tocopilla city</i>		
Norgener power plant (277 MW) ^a	5800	8911
Electroandina power plant (269 MW) ^a	10,146	18,357
On-road automobiles ^b	94	1
Port activities ^c	1653	
<i>Calama city</i>		
On-road automobiles ^b	619	8
<i>Inland smelters</i>		
Chuquicamata ^d		212,000
Noranda ^d		40,000
Antofagasta region (126,049 km ²) ^e	35,718	242,253
<i>Tarapacá bay (Tarapacá region)</i>		
Celta power plant (158 MW) ^a	3304	5075

^a Norgener and Electroandina data from [Jorquera \(2009\)](#), the other power plant data scaled from Norgener data based on their output shown in the parentheses.

^b Antofagasta data from [MMA \(2011\)](#), the others scaled from Antofagasta data based on the population relative to Antofagasta population (2008 population, Mejillones: 10,108; Antofagasta: 354,372; Tocopilla: 22,464; Calama: 147,702, [Lagos and Blanco, 2010](#)).

^c Tocopilla data from [Jorquera \(2009\)](#), Antofagasta data scaled from Tocopilla data based on the maximum loading ratio of 1676 to 480 million metric tons.

^d [Huneus et al., 2006](#).

^e [MMA, 2011](#).

primary aerosol production. NO₃⁻ in the deep ocean can exceed 30 ppm, but it is consumed as a nutrient by phytoplanktons in the euphotic zone, leading to surface water concentrations that are usually below detection limits ([Whitney and Freeland, 1999](#)). Therefore, primary sea-salt aerosols sourced from the ocean surface do not contain appreciable NO₃⁻. Instead, nitrogen oxides (NO_x = NO + NO₂) can be emitted from the ground (discussed below) to the atmosphere, where the majority of NO_x is then oxidized to HNO₃ ([Seinfeld and Pandis, 2006](#)). HNO₃ can then react on aerosols, including sea-salt particles containing Cl⁻, forming particulate NO₃⁻, which is ultimately deposited via dry and wet deposition ([Mamane and Gottlieb, 1992](#); [Zhuang et al., 1999](#)). The secondary NO₃⁻ produced should have accounted for the remainder of the NSS sulfate corrected Cl⁻ deficit at T1 site. The equivalent sum of the NSS SO₄²⁻ and NO₃⁻, called “acid equivalent” below, was: $2 \times R[\text{NSS SO}_4^{2-}] + R[\text{NO}_3^-] = 19.7 \text{ mmol m}^{-2} \text{ yr}^{-1}$. This actually exceeded the equivalent of the Cl⁻ loss by $1.8 \text{ mmol m}^{-2} \text{ yr}^{-1}$ and meant that

atmospheric H₂SO₄ and HNO₃ had the potential to displace more sea-salt Cl⁻ than what was observed. This did not occur, probably due to the presence of NH₃ and CaCO₃, which can buffer mineral acids (discussed below) in the atmosphere ([Ziereis and Arnold, 1986](#); [Evans et al., 2004](#)).

Sources of NO_x that produce NO₃⁻ include several anthropogenic and natural sources. Anthropogenic NO_x sources include fossil fuel combustion via electric generating units (EGUs), automobiles, and port activities. Natural sources of NO_x include nitrification, denitrification, stratospheric mixing and lightning ([Holland et al., 1999](#); [Galloway et al., 2004](#)). The preindustrial inorganic nitrogen deposition in the tropical and Southern Hemisphere temperate deserts of $\sim 2.9 \text{ mmol m}^{-2} \text{ yr}^{-1}$ ([Holland et al., 1999](#)) was adopted for that in the Atacama Desert, roughly half of it in the form of nitrate, *i.e.* $\sim 1.4 \text{ mmol NO}_3^- \text{ m}^{-2} \text{ yr}^{-1}$. This was in agreement with the estimate for remote ocean islands and south Pacific surface waters by [Duce et al. \(1991\)](#) and [Warneck \(2000\)](#). This suggested that the remaining $2.1 \text{ mmol m}^{-2} \text{ yr}^{-1}$ of atmospheric nitrate deposited at T1 site was of anthropogenic origin, which was supported by nitrate nitrogen and oxygen isotope evidence (discussed below). The anthropogenic nitrate was likely derived mainly from the nearby urban NO_x emissions from the Mejillones Peninsula and the city of Antofagasta that amounted to 15,200 metric tons NO_x per year ($4.0 \times 10^8 \text{ mol yr}^{-1}$) (Table 4). These anthropogenic NO_x emissions were 2.3 times higher than the coastal anthropogenic SO₂ emissions, but the anthropogenic NO₃⁻ deposition was only 0.3–0.6 of anthropogenic SO₄²⁻ deposition. This could be due to an overestimation of natural NO₃⁻ deposition, an overestimation of anthropogenic SO₄²⁻ in the trap, or long-distance transport of inland SO₂ or SO₄²⁻ to the T1 site, or a combination of all three.

The NH₄⁺ deposition rate at T1 site was second highest among the nine sites and should have provided a buffering capacity that partially explained the excess acid equivalents over the Cl⁻ loss. After being released from the land surface to the atmosphere, NH₃ has a short residence time of only a few hours and mostly deposits to the source region within 50 km ([Ferm, 1998](#)). Because of its high solubility, some NH₃ is hydrated to ammonium hydroxide that can be deposited back to the surface with wet deposition ([Renard et al., 2004](#)). More importantly, as the dominant atmospheric gaseous base, NH₃ rapidly reacts forming hygroscopic ammonium salts ([Ziereis and Arnold, 1986](#); [ApSimon et al., 1987](#)); typically, the (NH₄)₂SO₄, with a low NH₃ vapor pressure, is preferably formed compared to the NH₄NO₃. At T1 site, the NH₄⁺ deposition rate was $0.18 \text{ mmol m}^{-2} \text{ yr}^{-1}$, which would indicate that only a small amount of NH₃ had reacted with atmospheric acids and accounted for only a small portion of the imbalance between the potential acidity and Cl⁻ loss. Given the estimated imbalance of $1.8 \text{ mmol m}^{-2} \text{ yr}^{-1}$ and a base equivalent from NH₃ of $0.18 \text{ mmol m}^{-2} \text{ yr}^{-1}$, there would still be a $1.6 \text{ mmol m}^{-2} \text{ yr}^{-1}$ of the acid equivalent unbalanced.

The source of the NH₄⁺ at T1 site could be related to both natural system emissions and anthropogenic activities. It is well accepted that modern agricultural systems,

especially animal farming and fertilizer application, may have given rise to large losses of NH_3/NH_4 (NH_x) to the atmosphere (Bouwman et al., 1997). Considering the Atacama is generally barren, these land based natural sources cannot be a significant NH_3 contributor. Power plants in coastal cities (Mejillones, Antofagasta and Tocopilla) can also emit significant amounts of NH_3 , while other industrial processes and on-road automobile emissions are relatively minor. The NH_3 emissions from power plants were $\sim 1/9$ of the NO_x emissions in the Antofagasta region (MMA, 2011), suggesting that a significant fraction of NH_3 may have been from anthropogenic emissions. One potential natural NH_3 source is the upper ocean where NH_3 , produced during biological decomposition of organic matter by free-living bacteria or zooplankton (Kirchman, 2000), can exchange across the ocean/atmosphere surface (Quinn et al., 1996). The magnitude of this emission depends on the differences in NH_3 concentrations between in the atmosphere and ocean. Quinn et al. (1988, 1990) estimated a net flux of ammonia from the ocean to the atmosphere ranging between 0.7 and $5.8 \text{ mmol m}^{-2} \text{ yr}^{-1}$ in the central and Northeastern (NE) Pacific Ocean based on the measurements of NH_3 concentrations in the seawater and atmosphere. Clarke and Porter (1993) found that ammonium concentrations in aerosols were associated with seawater chlorophyll and had a similar net ocean to atmosphere flux of $3.6 \text{ mmol m}^{-2} \text{ yr}^{-1}$ over the equatorial Pacific. Despite T1 site being located along coastal Chile's highly productive upwelling zone, which has high ammonium regeneration rates (Probyn, 1987; Farras et al., 1996), our observed NH_4^+ deposition rate ($0.18 \text{ mmol m}^{-2} \text{ yr}^{-1}$) was surprisingly low. Liss and Galloway (1993) indicated that the oceanic ammonia fluxes should be similar to DMS fluxes, but our NH_4^+ deposition rate was at least seven times lower than the DMS-derived NSS SO_4^{2-} at T1 site. The $\text{NH}_4^+ / (\text{NSS } \text{SO}_4^{2-})$ was 0.02 , considerably lower than the $\text{NH}_4^+ / \text{SO}_4^{2-}$ molar ratios of 0.2 – 0.8 in remote marine aerosols in the equatorial Pacific measured by Clarke and Porter (1993). However, the observed NH_4^+ deposition at T1 site was consistent with an estimated dry deposition NH_4^+ flux of $0.18 \text{ mmol m}^{-2} \text{ yr}^{-1}$ in the NE Pacific Ocean (Quinn et al., 1988) and the bulk deposition NH_4^+ rate of $0.16 \pm 0.07 \text{ mmol m}^{-2} \text{ yr}^{-1}$ $\sim 120 \text{ km}$ southeast of T1 site in the Atacama (Ewing et al., 2006). This low NH_4^+ deposition rate was unlikely due to post-depositional nitrification of NH_4^+ in the trap based on the nitrate isotopes discussed below. The low rate was probably because free gaseous NH_3 accounted for $\sim 70\%$ of the total NH_3/NH_4 in the coastal atmosphere (Tsunogai, 1971; Yamamoto et al., 1995) and it was not efficiently retained by the inert surface of the dust trap. We conclude that only a small fraction of atmospheric NH_3 has neutralized atmospheric acids to form NH_4^+ , suggesting the preferable uptake of atmospheric acids by other atmospheric bases at T1 site.

4.1.4. Ca^{2+} excess at the T1 site

The large EF_{Na} for soil Ca^{2+} of 7.8 in the T1 trap suggested that there were other calcium sources in addition to dissolved seawater Ca^{2+} . The Ca^{2+} excess (e.g. non-sea-salt $\text{Ca}^{2+} = \text{NSS } \text{Ca}^{2+}$) could come from other major calcium

sources that include marine aerosols, weathering of parent material, and surface material. Silicate weathering has been considered a minor calcium source in the Atacama (Rech et al., 2003). Since there were no salt playas within 80 km of T1 site, the NSS Ca^{2+} in atmospheric dust at T1 site likely originated from oceanic inputs, including microorganisms with calcified shells, such as Coccolithophorids. Coccolithophorids are a characteristic group of mostly unicellular algae with delicate calcified scales and significant contributors to the phytoplankton community in the South America coastal upwelling regions (Klavness and Paasche, 1979; Chavez and Barber, 1987). The CaCO_3 scales can continually slough off as the Coccolithophorids grow or are released during viral infection or predation. These scales may mainly accumulate in the ocean's surface microlayer (upper 0 – 1 mm) (Hardy, 1982) and then readily inject into the atmosphere to form marine aerosols (MacIntyre, 1974; Fitzgerald, 1991), which may have led to the observed NSS Ca^{2+} in the T1 trap. Similar observations of marine aerosol NSS Ca^{2+} sourced off coastal New Zealand were attributed to biological surface Ca^{2+} fluxes (Sievering et al., 2004), and our observed $\text{Ca}^{2+} \text{EF}_{\text{Na}}$ of 7.8 was in line with the EF_{Na} for NSS Ca^{2+} (4.6 – 27.0) in that study. Therefore, it could be concluded that all of the Ca^{2+} deposited at T1 site could be attributed to the ocean, i.e. the seawater and phytoplankton. This gave a sea-salt Ca^{2+} deposition rate of $0.53 \text{ mmol m}^{-2} \text{ yr}^{-1}$ and a NSS Ca^{2+} deposition rate of $3.57 \text{ mmol m}^{-2} \text{ yr}^{-1}$ ($\text{R}[\text{NSS } \text{Ca}^{2+}] = (\text{EF}_{\text{Na}}(\text{Ca}^{2+}) - 1) \times \text{R}[\text{Ca}^{2+}] / \text{EF}_{\text{Na}}(\text{Ca}^{2+})$).

If all the NSS Ca^{2+} originated from biogenic derived CaCO_3 , this could account for the slightly positive charge surplus and could further resolve the potential acidity- $[\text{Cl}^-]_{\text{loss}}$ disparity at T1 site. Generally, the seawater-derived alkalinity could be determined by $0.005 \times \text{R}[\text{Na}^+]$ (Millero, 1974) of $0.12 \text{ mmol m}^{-2} \text{ yr}^{-1}$. This alkalinity could be rapidly consumed during the oxidation of SO_2 or NO_x occurring on the sea-salt aerosols (Chameides and Stelson, 1992). However, the presence of other alkaline species, such as NH_3 or CaCO_3 , could help neutralize atmospheric acids. If assuming all NSS Ca^{2+} in the form of CaCO_3 , the alkalinity equivalent of NSS Ca^{2+} was $7.14 \text{ mmol m}^{-2} \text{ yr}^{-1}$, which far exceeded the unbalanced acid equivalent of $1.8 \text{ mmol m}^{-2} \text{ yr}^{-1}$ remaining after removing chloride displacement reactions. This was in line with the near-neutral pH value of the dust at T1 site despite the high amounts of acidic NSS and NO_3^- (Table 2). The neutralization of atmospheric acids on CaCO_3 or NaCl aerosols may have accounted for the low NH_4^+ deposition rate at T1 site. The Ca^{2+} deposition rate ($4.10 \text{ mmol m}^{-2} \text{ yr}^{-1}$) was comparable to the natural sulfate (seawater $\text{SO}_4^{2-} + \text{natural NSS } \text{SO}_4^{2-}$) of 2.7 – $5.9 \text{ mmol m}^{-2} \text{ yr}^{-1}$. This suggested that, in the absence of human sulfur emissions, sea-salt aerosols sourced off northern Chile would contain high amounts of CaSO_4 , but little CaCO_3 because of the NSS SO_4^{2-} reactions. Transport of these aerosols inland and their deposition may have contributed to widespread CaSO_4 (anhydrite) or $\text{CaSO}_4 \cdot 2\text{H}_2\text{O}$ (gypsum) mineral crusts observed in surface soils across the hyper-arid core of the Atacama (Erickson, 1981; Rech et al., 2003). Any sulfur excess, either from volcanic SO_2 emissions or increased DMS, would result in

$\text{Ca}^{2+}/\text{SO}_4^{2-}$ variations and a shift towards the production of other sulfate minerals, such as thenardite (Na_2SO_4), typically found in the subsurface of the Atacama soils.

4.1.5. Mg^{2+} and K^+ sources at the T1 site

The depletion of Mg^{2+} ($\text{EF}_{\text{Na}}: 0.5$) was difficult to explain with any natural Mg^{2+} losses or anthropogenic processes. Mg^{2+} can randomly substitute for Ca^{2+} to form Mg-calcite (CaCO_3) (Gattuso and Buddemeier, 2000; Andersson et al., 2008), and thus a Mg^{2+} excess was expected, but our observation contradicted this. We are arguing that the Mg^{2+} depletion was not a result of Na^+ enrichment by soil entrainment, since by assuming Mg^{2+} was representative of seawater, half of the Na^+ ($12.9 \text{ mmol m}^{-2} \text{ yr}^{-1}$) would have to come from soil. However, this assumption was unreasonable due to the negligible Na^+ concentration in the surrounding soil profiles (see discussion above). Instead, one possible interpretation was Mg^{2+} -involved unknown reactions inside the collecting pan. There was some hard, white material that could not be dissolved or washed from the trap screen and may have been insoluble MgCO_3 or $\text{Mg}(\text{OH})_2$. The highly saline environments and moisture (fog) in the T1 trap may have promoted this reaction since the same material was not observed in the other traps where fog incursions are rare. However, Sievering et al. (2004) also reported a similar Mg^{2+} deficit relative to Na^+ , but it was attributed to additional Na^+ inputs from the soil and glass fiber filters. We could not rule out some other unknown natural Mg^{2+} loss processes.

There was an EF_{Na} of K^+ (1.8) that must also have had origins other than seawater K^+ . The slight enrichment of K^+ in the T1 trap compared to seawater was not likely from natural biomass fuel use, or open burning of vegetation, since this did not occur in the arid, non-vegetative environment near T1 site (Didyk et al., 2000). Also, the K^+ excess was not likely due to the contribution from local soil K^+ because of the low content of K^+ in the soil as discussed above. Therefore, the K^+ excess may have been of anthropogenic origins, such as the fossil fuel burning or industry activities.

4.1.6. The role of wet deposition in ion accumulation at the T1 site

Wet deposition is the removal of atmospheric gases and particles by precipitation consisting of in-cloud and below-cloud scavenging and this may have been important at T1 site. While there was nearly no rainfall at T1 site (Houston, 2006), high-altitude terrains ($>500 \text{ m}$ elevation) can intercept low clouds to produce fogs, locally called “camanchaca”. These camanchaca may form every day in the winter and twice a day during the summer at some places because of high humidity, cold ocean surface waters, and widespread nuclei from salts and kelp (Schemenauer et al., 1988). Fog deposition rates along the Atacama’s coast have been reported (8.26 and $1.43 \text{ L m}^{-2} \text{ day}^{-1}$ at two sites 80 and 350 km south of T1 site, respectively) (Kidron, 1999; Larrain et al., 2002), but they were much higher than predicted surface deposition rates because of their fog collector design. These collectors were oriented vertically and collected fog proportionally to the horizontal

wind component (Schemenauer and Cereceda, 1994). Surface fog deposition, on the other hand, was mainly a function of the fog droplet fall velocities that are typically $1\text{--}5 \text{ cm s}^{-1}$ (Fuzzi et al., 1985; Garreaud and Muñoz, 2005), considerably lower than the horizontal wind speeds. If the fog liquid water content at T1 site was assumed to be 0.1 g m^{-3} , a typical water content for stratocumulus (Schemenauer and Isaac, 1984; Schemenauer and Joe, 1989), then the flux of fog water to the ground would be the product of fog droplet fall velocity and the liquid water content, giving a fog deposition rate of $1\text{--}5 \text{ mg m}^{-2} \text{ s}^{-1}$. This rate was similar to an observed fog deposition rate of $2.2 \text{ mg m}^{-2} \text{ s}^{-1}$ measured using a flat-funnel device (Fuzzi et al., 1985), similar to our collection trap orientation. With a foggy day frequency of $\sim 70\%$ (256 days per year) (Schemenauer et al., 1988; Cereceda and Schemenauer, 1991; Cereceda et al., 2008) and lasting for 8 h a day, the annual fog deposition at T1 site could then range from 7 to $37 \text{ L m}^{-2} \text{ yr}^{-1}$ (equivalent to $0.7\text{--}3.7 \text{ cm}$ annual precipitation), in line with the fog deposition rate of $25 \text{ L m}^{-2} \text{ yr}^{-1}$ estimated using the eddy covariance method at Cerro Guanaco (300 km to the north of T1 site) (Westbeld et al., 2009). Given this volume, the ion deposition rates at T1 site may have been greatly impacted by the fog deposition.

Estimates of the fog ion deposition rates at T1 could be derived if the ion concentrations of the fog were known. Multiplication of the median fog deposition rate ($22 \text{ L m}^{-2} \text{ yr}^{-1}$) and the ion concentrations in two coastal fogs (El Tofo and Grande fogs) (Table 5) gave conflicting rates. The ion deposition rates based on the Grande fog ion concentrations were 13–30 times higher than the total deposition in the T1 trap. In particular, the Grande fog was considerably more enriched in Ca^{2+} than El Tofo fog (67-fold), and had a $\text{Ca}^{2+}/\text{SO}_4^{2-}$ molar ratio of ~ 1 similar to gypsum minerals found on the Salar de Grande’s surface, near where the fog was collected. The NO_3^- concentration in Grande fog was 25.4 times in El Tofo fog, and six times higher compared to the T1 trap, suggesting the Grande fog may have been subject to anthropogenic NO_x emissions from the nearby Tocopilla city and Tarapacá power plants (Table 4). This indicated that Grande fog ion content was considerably impacted by the dust from Salar de Grande and anthropogenic emissions and it would not be suitable for the comparison with the T1 trap sample. The El Tofo fog had a similar ionic composition to the T1 trap as shown by EF_{Na} (Table 3) despite small discrepancies in Ca^{2+} , Mg^{2+} and Cl^- (Schemenauer and Cereceda, 1992). Using the El Tofo fog ion content as the basis, the fog Na^+ deposition rate at T1 site was $4.6 \text{ mmol m}^{-2} \text{ yr}^{-1}$, which was 20% of the total Na^+ deposition rate ($23.9 \text{ mmol m}^{-2} \text{ yr}^{-1}$). The Cl^-/Na^+ molar ratio of 1.06 in the El Tofo fog ($\text{EF}_{\text{Na}}: 0.9$, Tables 3 and 5) indicated that there was nearly no Cl^- deficit in the El Tofo fog (the same EF_{Na} of 0.9 for the Grande fog). This was likely because displaced $\text{HCl}_{(\text{g})}$ in the air column could be scavenged by the fog. This scavenging would not be apparent in the T1 trap because the dissolved HCl would volatilize upon evaporation of the fog water. The fog Ca^{2+} deposition rate at El Tofo was estimated of $0.5 \text{ mmol m}^{-2} \text{ yr}^{-1}$, 10% of that in T1 trap sample, and its EF_{Na} of 5.2 was also lower than the EF_{Na}

Table 5

The ion composition of fog, lake and snow water samples and the derived ion deposition rates.

Samples	NH ₄ ⁺	Ca ²⁺	K ⁺	Mg ²⁺	Na ⁺	Cl ⁻	NO ₃ ⁻	SO ₄ ²⁻
<i>Ion concentration, μmol L⁻¹</i>								
El Tofo fog ^a	65.0	24.0	9.5	25.8	209.1	221.7	32.7	95.0
Grande fog	n.d.	1621.2	272.0	392.6	3397.9	3546.7	831.1	1406.2
Tara lake water	n.d.	1014.3	153.0	95.7	9935.7	10630.9	0.0	215.6
Tara snow	n.d.	106.3	24.5	14.0	324.0	186.7	10.8	70.9
Cerro Tapado snow ^b	2.8	4.2	0.5	0.9	2.9	3.0	5.7	4.8
El Tatio snow ^c	n.d.	28.5	9.5	5.0	87.0	140.8	n.d.	31.3
<i>Fog ion flux, mmol m⁻² yr⁻¹ with the fog deposition rate of 22 L m⁻² yr⁻¹</i>								
El Tofo fog	1.4	0.5	0.2	0.6	4.6	4.9	0.7	2.1
Grande fog	n.d.	35.7	6.0	8.6	74.8	78.0	18.3	30.9
<i>Snow ion flux, mmol m⁻² yr⁻¹ with the snow deposition rate of 50 mm yr⁻¹</i>								
Tara snow	n.d.	5.3	1.2	0.7	16.2	9.3	0.5	3.5
Cerro Tapado snow	0.4	0.2	0.0	0.0	0.1	0.1	0.3	0.2
El Tatio snow	n.d.	1.4	0.5	0.3	4.3	7.0	n.d.	1.6

n.d. – not determined.

^a El Tofo (29.26°S, 71.15°W, elevation: 780 m, 34 km away from the ocean) (Schemenauer and Cereceda, 1992).^b Cerro Tapado (30.13°S, 69.92°W, 5536 m asl, 800 km south of T10 site) (Ginot et al., 2001).^c El Tatio (22.37°S, 68.00°W, 4345 m asl, 100 km northwest of T10 site) (Houston, 2007).

of 7.8 for Ca²⁺ for T1 trap sample, which was probably related to the smaller number of the Coccolithophorids at the latitude of El Tofo site compared to of our T1 site in South Pacific (Saavedra-Pellitero et al., 2010). The EF_{Na} for SO₄²⁻ in El Tofo fog of 7.5 was slightly higher than that of 6.6 for T1 trap sample. The significantly larger EF_{Na} for K⁺ and Mg²⁺ of the El Tofo fog as well as the Grande fog suggested that K⁺ and Mg²⁺ in fogs were more enriched than in the T1 trap sample, possibly because of K⁺ and Mg²⁺ minerals in local land surface material entrained and captured by the fog at these two fog sites. While the two fog samples were both subject to local entrainment and geographic influence, the estimated El Tofo fog ion deposition rates were likely more similar to the fog ion deposition rate at T1 site. This suggested that fog was an important pathway of atmospheric deposition at T1 (~20%) and even more efficient in scavenging gaseous species. However, given the uncertainties in estimating fog ion deposition using data from sites other than T1, future monitoring of T1 site fog deposition rates and fog water composition is warranted.

The fogs may enhance coastal deposition of large marine aerosols but may not significantly impact small particles' transport inland (sea salts, NSS Ca²⁺, and secondary NO₃⁻ and SO₄²⁻). Two mechanisms for marine aerosol removal are possible. The first is simply that the fogs are nucleated on aerosols that would predominately be large sea-salt aerosols along the coast, and the high frequency of fog events would result in high removal rates (Noone et al., 1992; Seinfeld and Pandis, 2006). The second mechanism is cloud processing, where small sea-salt particles accumulate in fog droplets as solutes but the droplets are not deposited. Upon evaporation, the salts crystallize forming larger aerosols relative to their initial state that can then be more effectively removed by gravitational settling (O'Dowd et al., 1998). The fogs, however, are typically occurring at low elevations (500–1000 m) (Cereceda et al.,

2002, 2008) and these two mechanisms would not be effective in removing particles high in the boundary layer and free troposphere. Small particles and gases, such as SO₂ derived from DMS and HNO₃, are more effectively mixed to the upper boundary layer and free troposphere (Ferek et al., 1986) and they would therefore be more efficiently transported inland. This would suggest that deposition of secondary aerosols generated over the ocean, particularly NSS SO₄²⁻, would be proportionately more important inland relative to the coast and that a significant fraction of the Atacama's sulfate deposits are a result of biogenic sulfur emissions (in the absence of human sulfur emissions).

4.2. Dust deposition rates and composition at the Andean site T10

The T10 site was located in a closed basin surrounded by rolling hills and a high-altitude lake (4260 m) on the Andean altiplano. The bulk dust deposition rate of 35.1 g m⁻² yr⁻¹ at T10 site was more than two times the rate at the other sites, and 92.7% of it was ascribed to sand-sized insoluble mineral particles. These were likely due to weathered mineral particles blowing in from the surrounding hills during frequent high winds. The ionic contents in the local surface soil (0–10 cm) at T10 site were low, 0.0005 mmol g⁻¹ Cl⁻, undetectable NO₃⁻ and 0.0004 mmol g⁻¹ SO₄²⁻ (preliminary data), yielding a potential deposition flux of 0.02 and 0.015 mmol m⁻² yr⁻¹ Cl⁻ and SO₄²⁻, respectively. This indicated that the local soil deposition contributed less than ~1% of Cl⁻, NO₃⁻ and SO₄²⁻ to Trap 10, suggesting that local soil surfaces exerted a negligible influence in the deposition of Cl⁻, NO₃⁻, SO₄²⁻, and other ions. Therefore, soil contribution to ionic deposition was not considered in the remainder of the discussion. The total salt deposition rate was relatively low (2.6 g m⁻² yr⁻¹) compared to T1, probably due to its distance from the ocean and the lack of anthropogenic pollution in this

remote, high-elevation region. However, the Andean weathering and long-distance transport from the easterly source could be unique material sources on the Andean altiplano that may have provided significant inputs to the atmospheric deposition at T10 site (Rech et al., 2003). Therefore, a detailed study of the atmospheric deposition at T10 site can be meaningful to identify the Andean signatures for atmospheric deposition that are potentially used to further determine the importance of Andean sources for the atmospheric deposition in the Atacama region.

The ionic charge was not balanced at T10 site (positive/negative charge ratio of 0.77), in contrast with the other sites. This indicated there may have been other positive-charged ions (iron and H^+ would be insufficient to account for the balance) or functional groups that were present in the soil but not detected by our measurements. Ion charge imbalance in deposition has also been observed by other studies in the Atacama (Schemenauer and Cereceda, 1992; Grosjean et al., 1995; Ewing et al., 2006). The T10 site was close to vegetation-covered soils that surround the Tara lake and may have been sources of organic matter and clays. Therefore, the charge imbalance at T10 site may have been due to the presence of negatively charged organic matter or clay minerals that could exchange cations during filtration.

4.2.1. The role of snow deposition at the T10 site

The T10 site was the wettest site, with the annual average precipitation of ~ 150 mm, and wet deposition could thus have accounted for a significant fraction of soluble ions at T10 site. However, during our 2007–2009 collection period, La Niña was in effect and precipitation was only approximately 50 mm, mainly as snow (DGA, 2010). In order to constrain the importance of snow in ion deposition at T10 site, ion concentrations in three regional snows were compared. The ion concentrations in a remnant snow drift (Tara snow) near T10 (except Cl^-) were considerably higher than in the El Tatio or Cerro Tapado snow (two fresh snow samples) (Ginot et al., 2001; Houston, 2007) (Table 5). This was probably because ion concentrations in snow drifts (Tara snow) were known to increase through snow sublimation. Therefore, Tara snow was excluded from our further comparison with the T10 trap data. The ionic concentrations (except NO_3^-) in the Cerro Tapado snow were 5–47 times lower than in the El Tatio snow, which could be explained by the ion dilution effect occurring at Cerro Tapado site because of snow accumulation rates as high as ~ 1000 mm yr^{-1} (Ginot et al., 2001). Therefore, only snow from El Tatio, which has similar average annual precipitation to T10 site, was used to estimate wet ion deposition at T10 site (Houston, 2007). The snow deposition rates of Ca^{2+} , K^+ , Mg^{2+} and SO_4^{2-} could account for 66–92% of those deposition rates detected in T10 trap, while the snow deposition rates of Na^+ and Cl^- exceeded those in the T10 trap. It was unlikely that this was due to the local entrainment of salar salt minerals at El Tatio site (personal communication with Dr. John Houston). Rather, the T10 trap may not have effectively retained all snow deposition and there were uncertainties in estimating the total snow fall at the T10 site. This also highlighted the uncertainties in

using a composite sample collected during one season (December 1999–March 2000) to estimate the net snow deposition rates over a different 2.5-year period. However, similar ionic molar ratios in the El Tatio snow and the T10 trap indicate that the snow precipitation was likely an important contributor of ion deposition at T10 site.

4.2.2. Local ion sources at the T10 site

Local ion sources on the Andean altiplano could also impact the atmospheric deposition at T10 site. The Cl^- deposition rate at T10 site was 2.86 mmol m^{-2} yr^{-1} , the third largest among the nine sites, while the Na^+ deposition (2.20 mmol m^{-2} yr^{-1}) was the lowest. This apparent contradiction was a result of there being little Cl^- displacement on NaCl aerosols at T10 site. The lack of Cl^- displacement corroborated by smaller amounts of SO_4^{2-} deposition relative to the Central Valley/coast, negligible amounts of NO_3^- deposition, and a Cl^-/Na^+ molar ratio of 1.3. This suggested that anthropogenic NO_x and SO_2 produced in the Central Valley or on the coast were not effectively entrained into the Andean altiplano (see discussion below) and were not reacting with local NaCl particles.

The source of the NaCl deposited in the T10 trap was likely local, rather than influenced by oceanic transport as T1 Trap. Mountain ranges can greatly hinder the transport of sea-salt aerosols, which was evidenced by the pronounced attenuation of Cl^- deposition (by 87%) by the Coastal Range (Table 2). This suggested that the delivery of oceanic Cl^- over the Coastal Range (1–2 km in altitude), the Domeyko Range (~ 3 km in altitude) and the Andes front (~ 5 km in altitude) to the Andean altiplano located ~ 320 km away from the Pacific coast was likely negligible. T10 is near the Tara lake, part of a series of connected salt lakes in the region, whose ionic content was primarily Na^+ and Cl^- with Cl^-/Na^+ molar ratio of 1.1 (Table 5). Salt crusts surrounding the lake, as well as large desiccated sections, would likely be a major source of NaCl in T10 trap. This is consistent with Cl^-/Na^+ molar ratio in T10 trap of 1.3 being similar to the ratio in Tara lake water (of 1.1) and local halite minerals (of 1.0). This was also supported by the conjecture attributing increases in Cl^- in Andean ice cores to recycled Cl^- from salt lakes during desiccation cycles in high-altitude closed basins (Herrerros et al., 2009).

Attributing NaCl to the lake system contradicts the conclusion that snow can account for most of the NaCl. However, the high Cl^- concentrations in the El Tatio snow relative to similar mountain systems suggest that local NaCl is likely incorporated into snow. For example, the Cl^- concentrations in snow collected in the Sierra Nevada range (US) average 11.3 $\mu\text{mol L}^{-1}$ (Feth et al., 1964), nearly 10 times less than El Tatio snow. This is in spite of the fact that the Sierra Nevada and Andes are geographically similar, including distance to the ocean, coastal ocean circulation characterized by cold water upwelling zones, the barrier of a coastal range, and high altitude (Feth et al., 1964). Indeed, one would expect the higher elevation of the Andes to result in less Cl^- deposition because of rainout and particle settling. However, salt playas are common in the Central Andes but absent in the Sierra Nevada, which likely accounts for the difference in the Cl^- concentration in their

snow. Thus, it is likely that the high amount of NaCl found in the El Tatio snow was from local dust acting as cloud condensation nuclei or washed out during precipitation events. Therefore, it is unlikely that the salt lake and snow can be considered separate sources of ion deposition in T10 trap rather they are one and the same.

While the NaCl found in the T10 trap may originate from the Tara lake system, the $\text{SO}_4^{2-}/\text{Cl}^-$ molar ratio (0.8) was considerably higher than in the lake (0.2), suggesting there were additional source(s) of SO_4^{2-} other than the Tara Lake. There were two copper smelters that can provide SO_2 precursor gases for H_2SO_4 production in the Atacama region (Table 4) and the “Andean pump” effect could induce eastward air flows (Rutllant et al., 2013). However, the SO_4^{2-} deposition rate of $2.37 \text{ mmol m}^{-2} \text{ yr}^{-1}$ at T10 site was lowest among all nine sites, suggesting limited amounts of anthropogenic derived SO_4^{2-} have reached the high altitude site, which was also supported by apparent minimal Cl^- volatilization loss. The low anthropogenic SO_4^{2-} inputs were probably due to most SO_4^{2-} being pumped into the free troposphere and lost instead of being delivered to the Andean altiplano. Therefore, the SO_4^{2-} in T10 trap could not be mainly attributed to anthropogenic inputs, but is likely due to the local entrainment of surface, stream, lake, and salar salts (reflecting Andean weathering material) as suggested by Rech et al. (2003).

Total N deposition at T10 site was the lowest of all sites and reflected a relatively pristine environment that is not significantly impacted by Central Valley anthropogenic N emissions. The NO_3^- deposition rate at T10 site ($0.54 \text{ mmol m}^{-2} \text{ yr}^{-1}$) was a factor of 3–8 lower than at the other sites, and only 38% of model-estimated ($1.4 \text{ mmol m}^{-2} \text{ yr}^{-1}$) preindustrial nitrate deposition (Duce et al., 1991; Holland et al., 1999; Warneck, 2000). It was similar to wet deposition ($0.36 \text{ mmol m}^{-2} \text{ yr}^{-1}$) at a remote high-altitude site on the eastern slope of the Andes in southern Chile (Galloway et al., 1996), supporting the hypothesis that NO_3^- may have been primarily due to snow deposition. The NO_3^- was unlikely from local NO_x emissions (a single, low usage road) or NO_3^- minerals, since there were no reported nitrate-bearing playas or exposed nitrate minerals in the Andes region. Thus the low NO_3^- deposition rate has reflected limited regional emissions, the modern global nitrogen budget (Galloway et al., 2004), and the mountain crest effect because of material scavenging along the mountain slope (Feth et al., 1964). This was consistent with the minor importance of anthropogenic sulfur pollution in SO_4^{2-} deposition (discussed above). The NH_4^+ deposition rate ($0.19 \text{ mmol m}^{-2} \text{ yr}^{-1}$) was the highest of all sites and was likely the result of the local high-altitude prairie ecosystem with significant animal grazing and possibly the upwind Amazon plain where there is frequent biomass-burning activity (Andreae et al., 1988).

To sum up, the T10 site featured the largest insoluble dust deposition but lowest salt deposition rates among all sites. The salt ions (except NO_3^-) at T10 site mainly originated from the entrainment of local surface material (like salt lakes) or the snow deposition with salt components incorporated. In contrast, low NO_3^- and SO_4^{2-} deposition rates reflected a pristine environment with little anthropogenic

influence, but some delivery of SO_2 and NO_x emissions from the Central Valley. Considering the small amounts of salts at T10 site and the predominant eastward air flows, the net flux of salts from the Andean altiplano to the Central Valley should be small.

4.3. Dust deposition rates and composition at the inland sites T2–T8

The T2–T6 sites were located in the longitudinal depression (Central Valley) of the Atacama, bounded by the Coastal Range to the west and the Pre-Andes (separated by Domeyko Fault system from the Andes Range) to the east. The rain shadow effects created by these two mountain ranges make this central region the driest portion of the desert (<10 mm annual average precipitation), called the hyper-arid core of the Atacama Desert (Ericksen, 1981). The T7 and T8 sites were located on the Cordillera de Domeyko, and the rim of the Atacama basin (Salar de Atacama), respectively. These Pre-Cordillera sites were slightly wetter than the valley site with $\sim 10 \text{ mm}$ annual average precipitation (Houston, 2006). The atmospheric deposition at these seven inland sites is hypothesized to be impacted by a mixing of the oceanic and Andean inputs, local entrainment and anthropogenic emissions with essentially no wet deposition.

4.3.1. The attenuation of oceanic inputs over the Coastal Range

There was an abrupt decrease in the salt deposition rate from the T1 to T2 site, reflecting an efficient blocking of oceanic aerosol salts by the Coastal Range. The NH_4^+ , Na^+ , Cl^- and SO_4^{2-} deposition rates at T2 site dropped by 73%, 87%, 83% and 61%, respectively, relative to those at T1 site. This was comparable to the 90% attenuation of sea-salt particles by the 2000 m high coastal mountain range in Alaska (Shaw, 1991), and consistent with low Cl^- deposition in the lee of the Rocky Mountains in the US (Junge and Gustafson, 1957). This efficient removal of oceanic aerosol ions was likely related to scavenging by wet deposition (fog) and dry deposition of large sea-salt particles by gravitational settling on the windward side of the mountains (McDonald et al., 1982) as discussed above. The deposition rate of Mg^{2+} decreased by 37%, which could be doubled to 74%, similar to the decrease in Na^+ , Cl^- and SO_4^{2-} , if the missing Mg^{2+} in Trap 1 was due to aqueous reactions on the trap screen. In contrast, the deposition rates of Ca^{2+} and NO_3^- decreased only by 14% and 17%, respectively. Since most NH_4^+ , Na^+ , Cl^- , SO_4^{2-} , Mg^{2+} and NO_3^- salts have similar solubility, the lower attenuation of Ca^{2+} , NO_3^- , and possibly SO_4^{2-} , indicated there may have been significant sources of these latter ions other than marine aerosols at the T2 site.

4.3.2. The Andean inputs to the west of the Andes

Rech et al. (2003) suggested that Andean inputs are a significant source of material in the Central Valley and Pre-Andes region (T2–T8) but this was not supported by our data. The T10 site had the lowest ion deposition rates (except Cl^-) among all the nine sites, which were

specifically lower than at its nearest T8 site by 30–270%, suggesting small aerosol loadings at T10 site and scanty material that could be transported out of the Andes. This was probably because at T10 site, mineral dust from local entrainment can be quickly gravitationally settled and the Andean snow does not occur in low-altitude regions (Houston, 2006). Moreover, considering aerosol removal by the Pre-Andes range and the predominant westerly winds in the Atacama induced by the “Andean pump” effect, ion deposition west of the Andes was likely regulated by local entrainment of salts rather than Andean inputs. Therefore, though Rech et al. (2003) suggested that the Atacama Ca and S are a mixture of oceanic and Andean inputs, we are arguing that the Andean inputs are relatively minor to the west of the Andes. Indeed, the inland T2–T8 sites could likely be a source region for the Andean deposition such as SO_4^{2-} because of the westerly airflow as discussed above.

4.3.3. A comparison with previous research

The geographic location of the T2 site was similar to the Yungay site studied by Ewing et al. (2006) and a comparison of deposition characteristics between the two sites can give insights into local deposition effects. The Yungay site is located in a mountain basin to the east of the Coastal Range, 95 km to the south of the T2 site at a similar altitude (1276 m versus 1372 m for T2). The ion deposition rates at Yungay were 1.7–5.9-fold higher than those at T2 site (Table 2). However, the percentage of soluble/total material at the Yungay site ($37 \pm 22\%$) was similar to that at the T2 site (41.4%). This suggested that the Yungay site was subject to significantly more local dust deposition compared to our T2 site. This could not be evaluated, however, because the insoluble dust accumulation rate was not published (Ewing et al., 2006). A similar Cl^-/Na^+ molar ratio of 0.2 calculated based on their published data) and T2 (Cl^-/Na^+ molar ratio of 0.3) sites, revealing acid displacement on NaCl aerosols deposited at both sites (discussed above). The NH_4^+ deposition rate was similarly low at Yungay and T2, while the difference in the NO_3^- deposition rate by 5.9-fold between the two sites likely reflects the difference in total dust deposition. The Yungay's $\text{Ca}^{2+}/\text{SO}_4^{2-}$ molar ratio was only 0.32 compared to 0.96 at T2. Considering the ions at Yungay site were far from being charge balanced, it was difficult to infer the meaning of $\text{Ca}^{2+}/\text{SO}_4^{2-}$, which also limits a further comparison of the other ions between the two sites.

4.3.4. The impact of local entrainment and anthropogenic emissions at T2–T8 sites

After an abrupt decline in the Na^+ or Cl^- deposition rate from T1 to T2 site, these rates were relatively constant at T2–T8 sites. There was no clear trend of the Na^+ deposition rate with distance from the ocean, suggesting that Na^+ at T2–T8 sites was not exclusively from the oceanic inputs, but subject to some other sources. Though the most important source of inland Cl^- deposition may have been sea-salt, there are also salt playas containing chloride deposits (Stoertz and Erickson, 1974). For example, the relatively high Na^+ and Cl^- deposition rates at the T8 site could be explained by eolian input from the nearby Salar

de Atacama, the largest NaCl-type salt playa in Chile, while the second-highest Na^+ deposition rates at T5 site was likely attributed to the influence of Salar de Pampa Blanca (7.5 km to the southwest) that is rich in NaCl (Stoertz and Erickson, 1974). The Cl^-/Na^+ molar ratios at the T2–T8 sites were in the range of 0.2–0.7, indicating a chloride deficit relative to NaCl at these valley sites, which could be due to displacement by atmospheric acids and/or the enrichment of Na^+ . The $\text{Na}^+ / (\text{Cl}^- + \text{NO}_3^-)$ molar ratios of 0.94–1.26 approximated to 1 (Table 2), which supported the mechanism of Cl^- displacement by nitric acid or the enrichment of Na^+ in the form of NaNO_3 . We argue that the displacement reactions were more important, based on the common absence of NaNO_3 in the surface soil and on isotopic evidence (see detailed discussion below).

The NO_3^- deposition rate was relatively consistent in the range of 2.0–4.8 $\text{mmol m}^{-2} \text{yr}^{-1}$ at T2–T8 sites. This was comparable to 17 $\text{mmol m}^{-2} \text{yr}^{-1}$ if corrected by the several-fold higher total dust deposition at Yungay site. The NO_3^- deposition inland (T3, T5 and T6 sites) exceeded that of T1 and T2 sites (closest to the coastal urban regions), which could not be completely explained by the coastal anthropogenic inputs. Local entrainment of surface material may have also contributed to the trap NO_3^- deposition. Though there was a lack of NO_3^- in the upper 10 cm of most Atacama soil (preliminary data), there are many abandoned nitrate mines that have exposed subsurface nitrate minerals that could be sources of atmospheric nitrate. If true, then this would be most evident at the T5 site that was located in the Sierra Gorda nitrate works (Erickson, 1981) and near the Salar de Pampa Blanca that has surface crusts containing NaNO_3 (Stoertz and Erickson, 1974). However, isotopic evidence seemed to refute this explanation, though the T5 had the highest NO_3^- concentration among the nine sites. Modern secondary atmospheric NO_3^- had $\Delta^{17}\text{O}$ values of 20–32‰, and the T5 site had trap NO_3^- $\Delta^{17}\text{O}$ values of 25.6‰, within $\pm 0.7\%$ of the $\Delta^{17}\text{O}$ values at the T2–T8 sites. The Atacama surface NO_3^- , on the other hand, had $\Delta^{17}\text{O}$ values between 15‰ and 21‰ significantly lower than the traps values (Michalski et al., 2004). The consistently high NO_3^- $\Delta^{17}\text{O}$ values in the T2–T8 trap samples and the absence of a lower $\Delta^{17}\text{O}$ values in T5 trap NO_3^- suggested that soil NO_3^- entrainment was minimal. The T3 and T5 sites, with the highest NO_3^- deposition, were ~ 2 km away from major roads, while T6 site was 40 km away from the city of Calama, both of which emitted significant amounts of NO_x . This suggested that although we tried to minimize the potential anthropogenic influence at our sites, there were still significant anthropogenic activities across the Atacama that impact NO_3^- deposition. This was supported by relatively lower NO_3^- deposition at T7 and T8 sites, which are furthest from road and city NO_x sources.

The Ca^{2+} and SO_4^{2-} deposition rates were relatively consistent at T2–T8 sites (Table 2) with the $\text{Ca}^{2+}/\text{SO}_4^{2-}$ molar ratio of 0.91 ± 0.12 . The comparable concentrations of Ca^{2+} and SO_4^{2-} suggested the deposition of CaSO_4 (anhydrite) or $\text{CaSO}_4 \cdot 2\text{H}_2\text{O}$ (gypsum) minerals as dust. These minerals may have been sourced from local soil entrainment considering they are widespread on the surface of Atacama soils and usually occur just below surface clasts

forming large polygonal surface structures (chuca layer) (Erickson, 1981; Rech et al., 2003). These surface minerals are susceptible to wind erosion and disturbance by off-road vehicles and surface mining (field observation), which would enhance regional entrainment CaSO_4 .

That surface gypsum may have been the dominant source of SO_4^{2-} at the T2–T8 sites was somewhat surprising given the amount of anthropogenic SO_4^{2-} emissions along the trap gradient (Table 4). In the Antofagasta region, which encompasses the traps, the total SO_2 emissions were $3.8 \times 10^9 \text{ mol yr}^{-1}$ and were dominated by the Chuquicamata copper smelter, the largest open-pit copper mine in the world, while NO_x ($x = 1.5$) emissions were $\sim 9.4 \times 10^9 \text{ mol yr}^{-1}$. Given a 1.5-fold higher SO_2 emission rate relative to NO_x in the Antofagasta region and assuming equal proportions of NO_x and SO_2 were converted to NO_3^- and SO_4^{2-} , we would expect four times as much SO_4^{2-} relative to NO_3^- . Yet the molar ratio was only 1.2 ± 0.3 . Thus it appeared that at least 75% of secondary aerosol SO_4^{2-} was not being deposited in the traps. Even this is a low estimate given that the $\text{Ca}^{2+}/\text{SO}_4^{2-}$ molar ratio indicated much of the SO_4^{2-} was local gypsum dust.

This low anthropogenic SO_4^{2-} deposition in the Central Valley could arise from several reasons. The chemical conversion of SO_2 into SO_4^{2-} was considerably slower than the oxidation of NO_x to NO_3^- (Seinfeld and Pandis, 2006). Therefore, transport of SO_2 out of the basin may have occurred faster than SO_4^{2-} production. This could be facilitated by the “Andean pump” effect which draws SO_2 eastward into the free troposphere. SO_2 oxidation may have also been hindered by the near absence of boundary layer clouds at T2–T8 sites. In the absence of clouds, the oxidation of SO_2 via OH radical in the gas phase ($\text{SO}_2 + \text{OH} + \text{M}(\text{N}_2, \text{O}_2) \rightarrow \text{HOSO}_2 + \text{M}$) is the only effective sulfate production pathway. The chemical lifetime (τ) of SO_2 would then be approximately: $1/\tau = k[\text{OH}]$ where k was the effective second-order rate constant ($4.1 \times 10^{-13} \text{ cm}^3 \text{ molecule}^{-1} \text{ s}^{-1}$ at 300 K at 2400 m) and $[\text{OH}]$ was assumed to be $1 \times 10^6 \text{ molecules cm}^{-3}$ (Lee et al., 1990; Seinfeld and Pandis, 2006). This yielded a chemical lifetime of $\tau = \sim 28$ days, sufficiently long for the transport of SO_2 out of the basin before its conversion to SO_4^{2-} and subsequent deposition. In contrast, the apparent higher fraction of anthropogenic SO_4^{2-} at T1 (and T10) may have been due to aqueous SO_2 oxidation in the frequent fogs (clouds), which would decrease the chemical lifetime of SO_2 and result in more NSS SO_4^{2-} deposition along the coast.

Despite the overall relatively low SO_4^{2-} deposition rate, the importance of proximity of the anthropogenic sulfur sources for SO_4^{2-} deposition, could be detected near the Chuquicamata smelter. The T6 trap, nearest to the Chuquicamata smelter ($\sim 50 \text{ km}$ to the north), had the highest SO_4^{2-} deposition rate among T2–T8 sites with the $\text{Ca}^{2+}/\text{SO}_4^{2-}$ and $\text{Na}^+(\text{Cl}^- + \text{NO}_3^-)$ molar ratios of 0.8 and 1.3, respectively. This suggested the existence of anthropogenic SO_4^{2-} that could account for the chloride deficit. However, the SO_4^{2-} deposition at T6 site exceeded that of other inland sites by only $0.31\text{--}1.35 \text{ mmol m}^{-2} \text{ yr}^{-1}$, indicating that even at T6 site the deposition of local anthropogenic SO_4^{2-} was limited. This was probably because the Chuquicamata

smelter is located to the north of our trap array and the prevailing eastward wind (Rutilant et al., 2013) may have restricted the transport of SO_2 and SO_4^{2-} southward to our traps. Overall, the contribution of anthropogenic SO_4^{2-} inputs to the T2–T8 sites did not appear to be the main SO_4^{2-} source, rather it is surface gypsum/anhydrite dust.

The Mg^{2+} deposition rate logarithmically declined with the distance from T1 to T10 site: $R[\text{Mg}^{2+}] = -0.25 \times \ln(\text{distance}) + 1.79$ ($R^2 = 0.94$). This was consistent with models and observations that showed oceanic aerosol deposition decreasing exponentially with increasing distance from the ocean (Slinn et al., 1982). This suggested that Mg^{2+} at these nine sites was of oceanic origin, mainly seawater Mg^{2+} . In contrast, the K^+ deposition rate had abruptly dropped from T1 to T2 site and then varied among T2–T8 sites ($0.31 \pm 0.13\%$). This could probably be explained by that K^+ comes more easily from crustal dust and biogenic sources than Mg^{2+} (Hoffman et al., 1974; Buat-Ménard, 1983; Andreae, 1983).

Surface type may have influenced atmospheric deposition at T2–T8 sites because of the local entrainment of surface material. Entrainment of surface material usually has a short residence time because of the rapid gravitational settlement of larger aerosols near the source, and thus the local surface is an important source of dust deposition. The development of desert pavements and/or gypsum crusts, both common in desert regions, can protect the underlying soil profile from wind erosion, and are key factors controlling the degree of local entrainment (Qu et al., 2001; Goudie and Middleton, 2006). The T8 site had the largest bulk dust deposition rate of $9.7 \text{ g m}^{-2} \text{ yr}^{-1}$ among the seven inland sites. This site had no desert pavements, but rather windy conditions and NaCl crusts. Similarly, sparse desert pavements and disturbed surfaces at T5 site may have contributed to the observed high deposition rate of bulk dust ($9.6 \text{ g m}^{-2} \text{ yr}^{-1}$) and certain ions, like Ca^{2+} and SO_4^{2-} . Conversely, the T7 site, which contained dense stone desert pavements, had the lowest bulk dust and salt deposition rates of the sites studied: 5.0 and $2.2 \text{ g m}^{-2} \text{ yr}^{-1}$, respectively. Vegetation can be effective in protecting soil from wind erosion like stone pavements by binding the soil particles (Wolfe and Nickling, 1993) and its emissions and/or decomposition may also impact the soil property and even the regional deposition. Among T2–T8 sites, T6 was the only site with seasonal shrubs, whose presence may have explained why this site had a relatively low bulk dust deposition rate but the highest ammonium deposition rates among the seven inland sites.

4.4. Atmospheric NO_3^- isotope variations

The observed $\delta^{15}\text{N}$ of the trap NO_3^- varied from 1.5% to 10.6% , which may have reflected shifts in the NO_x sources. Different anthropogenic and natural sources of NO_x have distinctive $\delta^{15}\text{N}$ signatures (Heaton, 1986; Elliott et al., 2007). For example, $\delta^{15}\text{N}$ values of NO_x from coal-fired EGUs range from $+9.0\%$ to $+12.6\%$ (Felix et al., 2012), while vehicle NO_x exhausts have $\delta^{15}\text{N}$ values in the range of $+3.7\%$ to $+5.7\%$ (Moore, 1977; Ammann et al., 1999;

Pearson et al., 2000) with significantly lower $\delta^{15}\text{N}$ values from -13‰ to $+2\text{‰}$ also reported (Heaton, 1990). In comparison to natural NO_x , $\delta^{15}\text{N}$ values of NO_x produced by lightning and biogenic emissions range from 0‰ to $+2\text{‰}$ (Hoering, 1957), and from -20‰ to -49‰ (Li and Wang, 2008), respectively. A $\delta^{15}\text{N}$ analysis of NO_3^- in a 300 year-old Greenland ice core indicated that biomass burning can induce high $\delta^{15}\text{N}$ values of NO_x ($+14.3\text{‰}$) while fossil fuel burning is associated with negative $\delta^{15}\text{N}$ values (Hastings et al., 2009). These distinguishable $\delta^{15}\text{N}$ signatures of NO_x can then be imprinted on atmospheric NO_3^- via the transfer of N atoms during the oxidation of NO_x to NO_3^- and the small N isotopic fractionation associated with this oxidation (Freyer, 1991). Because the trap NO_3^- was deposited over a 2.5-year period, any $\delta^{15}\text{N}$ changes arising from seasonal shifts in NO_x chemistry or sources should have been eliminated. Therefore, $\delta^{15}\text{N}$ values of NO_3^- in the traps should reflect the $\delta^{15}\text{N}$ of the NO_x sources that produced the NO_3^- .

The observed $\delta^{15}\text{N}$ values of the trap NO_3^- varied depending on the trap location, which can help resolve the sources of NO_3^- found in the dust traps. At T1 site, the NO_3^- $\delta^{15}\text{N}$ was $+8.5\text{‰}$ (Fig. 4), slightly lower than the $\delta^{15}\text{N}$ values of coal-fired EGU-derived NO_x (Felix et al., 2012). This supported our previous prediction that T1 trap NO_3^- was mainly derived from coastal power plant NO_x emissions and port activities whose NO_x $\delta^{15}\text{N}$ signatures should be similar since they burn similar fuels (Table 3), but also due to natural sources (*i.e.* lightning, biogenic emissions and biomass burning) that typically possess lower $\delta^{15}\text{N}$ signatures. The NO_3^- $\delta^{15}\text{N}$ value of $+7.1 \pm 0.6\text{‰}$ at T2 site was similar to that at T1 site, also indicating that the collected NO_3^- was still primarily NO_x transported inland from nearby coastal power plants. There was a decrease in the NO_3^- $\delta^{15}\text{N}$ values from T3 to T8 sites. This suggested a shift in $\text{NO}_x/\text{NO}_3^-$ sources away from EGU's to mobile NO_x sources associated with the city of Calama and the Chilean central highway. The NO_3^- $\delta^{15}\text{N}$ of $+10.6 \pm 0.2\text{‰}$ at T10 was close to the NO_3^- $\delta^{15}\text{N}$ values for preindustrial ice core NO_3^- (Hastings et al., 2009), suggesting a minor anthropogenic imprint at T10 site and possibly a significant amount of NO_x from biomass burning on the altiplano or the Amazon Plain to the east.

The concurrent analysis of stable oxygen isotopes (^{16}O , ^{17}O and ^{18}O) can be indicative of atmospheric chemistry that transforms NO_x into NO_3^- and can help constrain sources of NO_3^- along the trap array. For the majority of the processes on Earth, the abundances of the three different oxygen isotopes depend on the relative isotope mass differences. This is termed as “mass-dependent fractionation” and follows the rule in $\delta^{17}\text{O} - 0.52 \cdot \delta^{18}\text{O}$ (Thiemens, 2006). However, deviations from mass-dependent fractionation have been observed in photochemically produced NO_3^- that can be quantified by $\Delta^{17}\text{O} = \delta^{17}\text{O} - 0.52 \delta^{18}\text{O}$ (Thiemens, 1999; Miller, 2002). Limited measurements have indicated the $\Delta^{17}\text{O}$ of modern atmospheric NO_3^- in the range of $20\text{--}33\text{‰}$ in non-polar regions (*e.g.* Michalski et al., 2003; Morin et al., 2009; Costa et al., 2011). The magnitude of the NO_3^- $\Delta^{17}\text{O}$ value is a function of the $\Delta^{17}\text{O}$ of ozone (the main NO_x oxidant), the amount of NO oxidized by

O_3 , and the relative importance of three major pathways of nitric acid production in the atmosphere: the third body mediated OH oxidation of NO_2 , heterogeneous hydrolysis of N_2O_5 on wet aerosol surfaces, and hydrogen abstraction by NO_3 radicals (Michalski et al., 2003, 2011; Alexander et al., 2009). Thus, changes in NO_3^- $\Delta^{17}\text{O}$ values can be related to atmospheric N chemistry regarding NO_x oxidation.

The NO_3^- $\Delta^{17}\text{O}$ values differed significantly between T1 and T10 sites (27.8‰ and 24.0‰ , respectively), but were relatively consistent across the remainder sites, ranging from $25.8 \pm 0.5\text{‰}$. The NO_3^- $\Delta^{17}\text{O}$ value (27.8‰) in the T1 trap was the highest among the nine sites. This was likely because of an increase of the heterogeneous N_2O_5 pathway ($\text{N}_2\text{O}_5 + \text{H}_2\text{O} + \text{surface} \rightarrow 2\text{HNO}_3$), which had a higher contribution of oxidation by ozone leading to higher NO_3^- $\Delta^{17}\text{O}$ values (Michalski et al., 2003, 2011). The enhanced N_2O_5 pathway was probably because of high aerosol surface area from the coastal fogs and high amount of sea-salt aerosols (evidenced by the high salt load in the T1 trap). The limited amount of sunlight caused by thick stratus cloud decks and cool temperature from Peru Current's coastal upwelling may have also been a factor. The NO_3^- $\Delta^{17}\text{O}$ values at T2–T8 sites were significantly lower than at T1 site ($p < 0.01$). This was likely the result of a decrease in the importance of the N_2O_5 pathway because of a lower number density of sea-salt and fog particles and the penetration of increased sunlight that promotes the OH oxidation pathway. The T10 site had the lowest NO_3^- $\Delta^{17}\text{O}$ value most likely due to the small amount of NO_x and clean air at this altitude. It is improbable that the midrange $\Delta^{17}\text{O}$ values at T2–T8 sites were the result of the mixing of the high $\Delta^{17}\text{O}$ NO_3^- from the coastal regions and the low $\Delta^{17}\text{O}$ values of NO_3^- from the Andes, since that would require $\sim 80\%$ contribution from the Andean NO_3^- which was unlikely given the Andean site has by far the lowest NO_3^- deposition rate.

5. CONCLUSIONS

A west–east array of nine dust traps were analyzed to investigate the characteristics and spatial variations of modern atmospheric deposition across the Atacama. The coastal trap (T1) had the second-highest insoluble particle deposition rate, perhaps due to the surrounding mountain ranges, and the largest amount of soluble salts that were dominated by Na^+ , Cl^- , Ca^{2+} and SO_4^{2-} ions, mainly from oceanic inputs including seawater droplets, calcium carbonate mineral and dimethyl sulfide emissions. The T10 trap was located on the Andean altiplano and likely susceptible to the weathering material from the Andes, leading to its highest insoluble particle deposition rate. The soluble salt deposition rates at T10 site were relatively low due to the minimal delivery of oceanic material and anthropogenic influence. Instead, the soluble salt ions at T10 site were mainly ascribed to the local entrainment of surrounding salts and snow deposition. There were relatively consistent insoluble mineral particle and soluble salt deposition rates among T2–T8 sites. While oceanic aerosols were greatly attenuated because of the blockage of the coastal mountain ranges, they still accounted for the main source of “new

material” to the interior, *i.e.* net accumulation. The Andes, on the other hand, had limited importance on atmospheric material deposited in the inland regions to the west. Local entrainment and secondary aerosols then accounted for most of the material at T2–T8 sites and the majority of gross accumulation in the Central Valley. The $\text{NO}_3^- \delta^{15}\text{N}$ and $\Delta^{17}\text{O}$ indicated the shifts in NO_x sources from the coastal power plants to the road activity emissions at inland sites. In addition, the NO_3^- chemistry experienced decreasing contributions of the N_2O_5 pathway from west to east.

ACKNOWLEDGMENTS

This work was supported by the United States National Science Foundation Grant (EAR 0922114), Purdue Rare Isotope Measurement (PRIME) Laboratory, and Mineralogical Society of America Student Award in mineralogy and petrology. We thank Zane Gilbert, Darrell Schulze, Brenda Bowen and Raul Ochoa for assistance during sample collection and analysis. We are also grateful for Dr. John Houston’s contribution about Chilean precipitation information.

APPENDIX A. SUPPLEMENTARY DATA

Supplementary data associated with this article can be found, in the online version, at <http://dx.doi.org/10.1016/j.gca.2014.03.017>.

REFERENCES

- Alexander B., Hastings M., Allman D., Dachs J., Thornton J. and Kunasek S. (2009) Quantifying atmospheric nitrate formation pathways based on a global model of the oxygen isotopic composition ($\Delta^{17}\text{O}$) of atmospheric nitrate. *Atmos. Chem. Phys.* **9**, 5043–5056.
- Amit R., Lekach J., Ayalon A., Porat N. and Grodek T. (2007) New insight into pedogenic processes in extremely arid environments and their paleoclimatic implications—the Negev Desert, Israel. *Quatern. Int.* **162**, 61–75.
- Ammann M., Siegwolf R., Pichlmayer F., Suter M., Saurer M. and Brunold C. (1999) Estimating the uptake of traffic-derived NO_2 from ^{15}N abundance in Norway spruce needles. *Oecologia* **118**, 124–131.
- Anderson K., Wells S. and Graham R. (2002) Pedogenesis of vesicular horizons, Cima volcanic field, Mojave Desert, California. *Soil Sci. Soc. Am. J.* **66**, 878–887.
- Andersson A. J., Mackenzie F. T. and Bates N. R. (2008) Life on the margin: implications of ocean acidification on Mg-calcite, high latitude and cold-water marine calcifiers. *Mar. Ecol. Prog. Ser.* **373**, 265–273.
- Andreae M. O. (1983) Soot carbon and excess fine potassium: long-range transport of combustion-derived aerosols. *Science* **220**, 1148–1151.
- Andreae M. O., Browell E. V., Garstang M., Gregory G., Harriss R., Hill G., Jacob D., Pereira M., Sachse G. and Setzer A. (1988) Biomass-burning emissions and associated haze layers over Amazonia. *J. Geophys. Res.* **93**, 1509–1527.
- Andres R. J., Rose W. I., Kyle P. R., DeSilva S., Francis P., Gardeweg M. and Moreno-Roa H. (1991) Excessive sulfur dioxide emissions from Chilean volcanoes. *J. Volcanol. Geoth. Res.* **46**, 323–329.
- ApSimon H., Kruse M. and Bell J. (1987) Ammonia emissions and their role in acid deposition. *Atmos. Environ.* **21**, 1939–1946.
- Ayers G., Gillett R., Caine J. and Dick A. (1999) Chloride and bromide loss from sea-salt particles in Southern Ocean air. *J. Atmos. Chem.* **33**, 299–319.
- Bao H., Jenkins K. A., Khachatryan M. and Díaz G. C. (2004) Different sulfate sources and their post-depositional migration in Atacama soils. *Earth Planet. Sci. Lett.* **224**, 577–587.
- Böhlke J. K., Erickson G. E. and Revesz K. (1997) Stable isotope evidence for an atmospheric origin of desert nitrate deposits in northern Chile and southern California, USA. *Chem. Geol.* **136**, 135–152.
- Bouwman A., Lee D., Asman W., Dentener F., Van Der Hoek K. and Olivier J. (1997) A global high-resolution emission inventory for ammonia. *Global Biogeochem. Cycles* **11**, 561–587.
- Buat-Ménard P. (1983) Particle geochemistry in the atmosphere and oceans. In *Air-sea Exchange of Gases and Particles* (eds. P. S. Liss and W. G. N. Slinn). D. Reidel Publishing Company, Dordrecht, pp. 455–532.
- Calhoun J. A., Bates T. S. and Charlson R. J. (1991) Sulfur isotope measurements of submicrometer sulfate aerosol particles over the Pacific Ocean. *Geophys. Res. Lett.* **18**, 1877–1880.
- Capo R. C. and Chadwick O. A. (1999) Sources of strontium and calcium in desert soil and calcrete. *Earth Planet. Sci. Lett.* **170**, 61–72.
- Cereceda P. and Schemenauer R. S. (1991) The occurrence of fog in Chile. *J. Appl. Meteorol.* **30**, 1097–1105.
- Cereceda P., Osses P., Larrain H., Farias M., Lagos M., Pinto R. and Schemenauer R. (2002) Advective, orographic and radiation fog in the Tarapacá region, Chile. *Atmos. Res.* **64**, 261–271.
- Cereceda P., Larrain H., Osses P., Farias M. and Egaña I. (2008) The spatial and temporal variability of fog and its relation to fog oases in the Atacama Desert, Chile. *Atmos. Res.* **87**, 312–323.
- Chameides W. and Stelson A. (1992) Aqueous-phase chemical processes in deliquescent sea-salt aerosols: a mechanism that couples the atmospheric cycles of S and sea salt. *J. Geophys. Res.* **97**, 20565–20580.
- Chand D., Hegg D., Wood R., Shaw G., Wallace D. and Covert D. (2010) Source attribution of climatically important aerosol properties measured at Pajón (Chile) during VOCALS. *Atmos. Chem. Phys.* **10**, 10789–10801.
- Charlson R. J., Lovelock J. E., Andreae M. O. and Warren S. G. (1987) Oceanic phytoplankton, atmospheric sulphur, cloud albedo and climate. *Nature* **326**, 655–661.
- Chavez F. P. and Barber R. T. (1987) An estimate of new production in the equatorial Pacific. *Deep Sea Res. Pt. I* **34**, 1229–1243.
- Clarke A. D. and Porter J. N. (1993) Pacific marine aerosol: 2. Equatorial gradients in chlorophyll, ammonium, and excess sulfate during SAGA 3. *J. Geophys. Res.* **98**, 16997–17010.
- Cooke R. U. (1970) Stone pavements in deserts. *Ann. Ass. Am. Geogr.* **60**, 560–577.
- Costa A., Michalski G., Schauer A., Alexander B., Steig E. and Shepson P. (2011) Analysis of atmospheric inputs of nitrate to a temperate forest ecosystem from $\Delta^{17}\text{O}$ isotope ratio measurements. *Geophys. Res. Lett.* **38**, L15805.
- Dan J. and Yaalon D. (1982) Automorphic saline soils in Israel. *Catena Suppl.* **1**, 103–115.
- Dirección General de Aguas (DGA) (2010) Actualización de la Evaluación de la Disponibilidad de Recursos Hídricos para Constituir Derechos de Aprovechamiento en las Subcuencas Afluentes al Salar de Atacama. II region, Santiago, Chile (in Spanish).
- Didyk B. M., Simoneit B. R., Alvaro Pezoa L., Luis Riveros M. and Anselmo Flores A. (2000) Urban aerosol particles of Santiago, Chile: organic content and molecular characterization. *Atmos. Environ.* **34**, 1167–1179.

- Duce R., Liss P., Merrill J., Atlas E., Buat-Menard P., Hicks B., Miller J., Prospero J., Arimoto R. and Church T. (1991) The atmospheric input of trace species to the world ocean. *Global Biogeochem. Cycles* **5**, 193–259.
- Elliott E., Kendall C., Wankel S., Burns D., Boyer E., Harlin K., Bain D. and Butler T. (2007) Nitrogen isotopes as indicators of NO_x source contributions to atmospheric nitrate deposition across the midwestern and northeastern United States. *Environ. Sci. Technol.* **41**, 7661–7667.
- Ericksen G. (1981) Geology and origin of the Chilean nitrate deposits. *US Geol. Surv. Prof. Pap.*, 1188.
- Evans M. C., Campbell S. W., Bhethanabotla V. and Poor N. D. (2004) Effect of sea salt and calcium carbonate interactions with nitric acid on the direct dry deposition of nitrogen to Tampa Bay, Florida. *Atmos. Environ.* **38**, 4847–4858.
- Ewing S., Sutter B., Owen J., Nishiizumi K., Sharp W., Cliff S., Perry K., Dietrich W., McKay C. and Amundson R. (2006) A threshold in soil formation at Earth's arid-hyperarid transition. *Geochim. Cosmochim. Acta* **70**, 5293–5322.
- Ewing S., Michalski G., Thiemens M., Quinn R., Macalady J., Kohl S., Wankel S., Kendall C., McKay C. and Amundson R. (2007) Rainfall limit of the N cycle on Earth. *Global Biogeochem. Cycles* **21**, GB3009.
- Fariás L., Chuecas L. A. and Salamanca M. A. (1996) Effect of coastal upwelling on nitrogen regeneration from sediments and ammonium supply to the water column in Concepcion Bay, Chile. *Est. Coast. Shelf Sci.* **43**, 137–155.
- Felix J. D., Elliott E. M. and Shaw S. L. (2012) Nitrogen isotopic composition of coal-fired power plant NO_x : influence of emission controls and implications for global emission inventories. *Environ. Sci. Technol.* **46**, 3528–3535.
- Ferek R., Chatfield R. and Andreae M. (1986) Vertical distribution of dimethylsulphide in the marine atmosphere. *Nature* **320**, 514–516.
- Ferm M. (1998) Atmospheric ammonia and ammonium transport in Europe and critical loads: a review. *Nutr. Cycl. Agroecosys.* **51**, 5–17.
- Feth J. H., Rogers S. M. and Roberson C. E. (1964) Chemical composition of snows in the northern Sierra Nevada and other areas. *US Geol. Surv. Water Supply Pap.*, 1535.
- Fitzgerald J. W. (1991) Marine aerosols: a review. *Atmos. Environ.* **25**, 533–545.
- Freyer H. (1991) Seasonal variation of $^{15}\text{N}/^{14}\text{N}$ ratios in atmospheric nitrate species. *Tellus B* **43**, 30–44.
- Fuzzi S., Orsi G. and Mariotti M. (1985) Wet deposition due to fog in the Po Valley, Italy. *J. Atmos. Chem.* **3**, 289–296.
- Galloway J. N., Keene W. C. and Likens G. E. (1996) Processes controlling the composition of precipitation at a remote southern hemispheric location: Torres del Paine National Park, Chile. *J. Geophys. Res.* **101**, 6883–6897.
- Galloway J. N., Dentener F. J., Capone D. G., Boyer E. W., Howarth R. W., Seitzinger S. P., Asner G. P., Cleveland C., Green P. and Holland E. (2004) Nitrogen cycles: past, present, and future. *Biogeochemistry* **70**, 153–226.
- Garreaud R. and Muñoz R. C. (2005) The low-level jet off the west coast of subtropical South America: structure and variability. *Mon. Wea. Rev.* **133**, 2246–2261.
- Gattuso J. P. and Buddemeier R. W. (2000) Ocean biogeochemistry: calcification and CO_2 . *Nature* **407**, 311–313.
- Gerson R. and Amit R. (1987) Rates and modes of dust accretion and deposition in an arid region—the Negev, Israel. *Geol. Soc. London Spec. Publ.* **35**, 157–169.
- Ginot P., Kull C., Schwikowski M., Schotterer U. and Gäggeler H. W. (2001) Effects of postdepositional processes on snow composition of a subtropical glacier (Cerro Tapado, Chilean Andes). *J. Geophys. Res.* **106**, 32375–32386.
- Goudie A. S. and Middleton N. (2006) *Desert Dust in the Global System*. Springer, Heidelberg.
- Grosjean M., Geyh M. A., Messerli B. and Schotterer U. (1995) Late-glacial and early Holocene lake sediments, ground-water formation and climate in the Atacama Altiplano 22–24°S. *J. Paleolimnol.* **14**, 241–252.
- Hardy J. T. (1982) The sea surface microlayer: biology, chemistry and anthropogenic enrichment. *Prog. Oceanogr.* **11**, 307–328.
- Harkel M. T. (1997) The effects of particle-size distribution and chloride depletion of sea-salt aerosols on estimating atmospheric deposition at a coastal site. *Atmos. Environ.* **31**, 417–427.
- Hastings M., Jarvis J. and Steig E. (2009) Anthropogenic impacts on nitrogen isotopes of ice-core nitrate. *Science* **324**, 1288.
- Heaton T. (1986) Isotopic studies of nitrogen pollution in the hydrosphere and atmosphere: a review. *Chem. Geol.* **59**, 87–102.
- Heaton T. (1990) $^{15}\text{N}/^{14}\text{N}$ ratios of NO_x from vehicle engines and coal-fired power stations. *Tellus B* **42**, 304–307.
- Herreros J., Moreno I., Taupin J. D., Ginot P., Patris N., Angelis M. D., Ledru M. P., Delachaux F. and Schotterer U. (2009) Environmental records from temperate glacier ice on Nevado Coropuna saddle, southern Peru. *Adv. Geosci.* **22**, 27–34.
- Hoering T. (1957) The isotopic composition of the ammonia and the nitrate ion in rain. *Geochim. Cosmochim. Acta* **12**, 97–102.
- Hoffman E., Hoffman G. and Duce R. (1974) Chemical fractionation of alkali and alkaline earth metals in atmospheric particulate matter over the North Atlantic. *J. Rech. Atmos.* **8**, 675–688.
- Holland E. A., Dentener F. J., Braswell B. H. and Sulzman J. M. (1999) Contemporary and pre-industrial global reactive nitrogen budgets. *Biogeochemistry* **46**, 7–43.
- Houston J. (2006) Variability of precipitation in the Atacama Desert: its causes and hydrological impact. *Int. J. Climatol.* **26**, 2181–2198.
- Houston J. (2007) Recharge to groundwater in the Turi Basin, northern Chile: an evaluation based on tritium and chloride mass balance techniques. *J. Hydrol.* **334**, 534–544.
- Huneeus N., Gallardo L. and Ruttland J. (2006) Offshore transport episodes of anthropogenic sulfur in northern Chile: potential impact on the stratocumulus cloud deck. *Geophys. Res. Lett.* **33**, L19819.
- Jorquera H. (2009) Source apportionment of PM10 and PM2.5 at Tocopilla, Chile (22°05'S, 70°12'W). *Environ. Monit. Assess.* **153**, 235–251.
- Junge C. E. and Gustafson P. (1957) On the distribution of sea salt over the United States and its removal by precipitation. *Tellus* **9**, 164–173.
- Kaiser J., Hastings M. G., Houlton B. Z., Röckmann T. and Sigman D. M. (2007) Triple oxygen isotope analysis of nitrate using the denitrifier method and thermal decomposition of N_2O . *Anal. Chem.* **79**, 599–607.
- Keene W. C., Pszenny A. A., Galloway J. N. and Hawley M. E. (1986) Sea-salt corrections and interpretation of constituent ratios in marine precipitation. *J. Geophys. Res.* **91**, 6647–6658.
- Keene W. C., Sander R., Pszenny A. A. P., Vogt R., Crutzen P. J. and Galloway J. N. (1998) Aerosol pH in the marine boundary layer: a review and model evaluation. *J. Aerosol Sci.* **29**, 339–356.
- Khoder M. (2002) Atmospheric conversion of sulfur dioxide to particulate sulfate and nitrogen dioxide to particulate nitrate and gaseous nitric acid in an urban area. *Chemosphere* **49**, 675–684.
- Kidron G. J. (1999) Altitude dependent dew and fog in the Negev Desert, Israel. *Agric. Forest Meteorol.* **96**, 1–8.
- Kirchman D. L. (2000) Uptake and regeneration of organic nutrients by marine heterotrophic bacteria. In *Microbial*

- Ecology of the Oceans* (ed. D. L. Kirchman). John Wiley & Sons, New York, pp. 261–289.
- Klavness D. and Paasche E. (1979) Physiology of coccolithophorids. In *Biochemistry and Physiology of Protozoa*, vol. 1 (eds. M. Levandowsky and S. H. Hutner). Academic Press, New York, pp. 191–213.
- Lagos G. and Blanco E. (2010) Mining and development in the region of Antofagasta. *Resour. Pol.* **35**, 265–275.
- Larrain H., Velasquez F., Cereceda P., Espejo R., Pinto R., Osses P. and Schemenauer R. (2002) Fog measurements at the site “Falda Verde” north of Chañaral compared with other fog stations of Chile. *Atmos. Res.* **64**, 273–284.
- Lee Y. Y., Kao W. C. and Lee Y. P. (1990) Kinetics of the reaction hydroxyl + sulfur dioxide in helium, nitrogen, and oxygen at low pressure. *J. Phys. Chem.* **94**, 4535–4540.
- Lewis R. and Schwartz E. (2004) *Sea Salt Aerosol Production: Mechanisms, Methods, Measurements and Models—A Critical Review*. American Geophysical Union, Washington, DC.
- Li D. and Wang X. (2008) Nitrogen isotopic signature of soil-released nitric oxide (NO) after fertilizer application. *Atmos. Environ.* **42**, 4747–4754.
- Liss P. S. and Galloway J. N. (1993) Air-sea exchange of sulphur and nitrogen and their interaction in the marine atmosphere. In *Interactions of C, N, P and S Biogeochemical Cycles and Global Change* (eds. R. Wollast, F. T. Mackenzie and L. Chou). Springer, Berlin, pp. 259–281.
- MacIntyre F. (1974) Chemical fractionation and sea-surface microlayer processes. In *The Sea* (ed. E. D. Goldberg). John Wiley & Sons, New York, pp. 245–299.
- Mamane Y. and Gottlieb J. (1992) Nitrate formation on sea-salt and mineral particles—a single particle approach. *Atmos. Environ.* **26**, 1763–1769.
- Marandino C., De Bruyn W., Miller S. and Saltzman E. (2009) Open ocean DMS air/sea fluxes over the eastern South Pacific Ocean. *Atmos. Chem. Phys.* **9**, 345–356.
- Mather T., Tsanev V., Pyle D., McGonigle A., Oppenheimer C. and Allen A. (2004) Characterization and evolution of tropospheric plumes from Lascar and Villarrica volcanoes, Chile. *J. Geophys. Res.* **109**, D21303.
- McDonald R., Unni C. and Duce R. (1982) Estimation of atmospheric sea salt dry deposition: wind speed and particle size dependence. *J. Geophys. Res.* **87**, 1246–1250.
- McFadden L. D., Wells S. G. and Jercinovich M. J. (1987) Influences of eolian and pedogenic processes on the origin and evolution of desert pavements. *Geology* **15**, 504–508.
- Michalski G., Scott Z., Kabling M. and Thiemens M. (2003) First measurements and modeling of ^{17}O in atmospheric nitrate. *Geophys. Res. Lett.* **30**, 1870.
- Michalski G., Böhlke J. and Thiemens M. (2004) Long term atmospheric deposition as the source of nitrate and other salts in the Atacama Desert, Chile: new evidence from mass-independent oxygen isotopic compositions. *Geochim. Cosmochim. Acta* **68**, 4023–4038.
- Michalski G., Bhattacharya S. K. and Mase D. F. (2011) Oxygen isotope dynamics of atmospheric nitrate and its precursor molecules. In *Handbook of Environmental Isotope Geochemistry: Advances in Isotope Geochemistry* (ed. M. Baskaran). Springer-Verlag, Berlin, Heidelberg, pp. 613–635.
- Miller M. (2002) Isotopic fractionation and the quantification of ^{17}O anomalies in the oxygen three-isotope system: an appraisal and geochemical significance. *Geochim. Cosmochim. Acta* **66**, 1881–1889.
- Millero F. J. (1974) Seawater as a multicomponent electrolyte solution. In *The Sea* (ed. E. D. Goldberg). John Wiley & Sons, New York, pp. 3–80.
- Ministerio del Medio Ambiente (MMA) (2011) Reporte 2005–2009 del Registro de Emisiones y Transferencias de Contaminantes, Gobierno de Chile, Chile (in Spanish).
- Moore H. (1977) The isotopic composition of ammonia, nitrogen dioxide and nitrate in the atmosphere. *Atmos. Environ.* **11**, 1239–1243.
- Morin S., Savarino J., Frey M. M., Domine F., Jacobi H. W., Kaleschke L. and Martins J. M. (2009) Comprehensive isotopic composition of atmospheric nitrate in the Atlantic Ocean boundary layer from 65°S to 79°N. *J. Geophys. Res.* **114**, D05303.
- Muñoz R. (2008) Diurnal cycle of surface winds over the subtropical southeast Pacific. *J. Geophys. Res.* **113**, D13107.
- Navarro-Gonzalez R., Rainey F., Molina P., Bagaley D., Hollen B., de la Rosa J., Small A., Quinn R., Grunthaner F. and Caceres L. (2003) Mars-like soils in the Atacama Desert, Chile, and the dry limit of microbial life. *Science* **302**, 1018.
- Newberg J. T., Matthew B. M. and Anastasio C. (2005) Chloride and bromide depletions in sea-salt particles over the northeastern Pacific Ocean. *J. Geophys. Res.* **110**, D06209.
- Noone K. J., Ogren J. A., Hallberg A., Heintzenberg J., Ström J., Hansson H. C., Svenningsson B., Wiedensohler A., Fuzzi S. and Facchini M. C. (1992) Changes in aerosol size-and phase distributions due to physical and chemical processes in fog. *Tellus B* **44**, 489–504.
- O’Dowd C. D. and de Leeuw G. (2007) Marine aerosol production: a review of the current knowledge. *Phil. Trans. Roy. Soc. A* **365**, 1753–1774.
- O’Dowd C. D., Geever M., Hill M. K., Smith M. H. and Jennings S. G. (1998) New particle formation: nucleation rates and spatial scales in the clean marine coastal environment. *Geophys. Res. Lett.* **25**, 1661–1664.
- Pearson J., Wells D., Sellar K., Bennett A., Soares A., Woodall J. and Ingrouille M. (2000) Traffic exposure increases natural ^{15}N and heavy metal concentrations in mosses. *New Phytol.* **147**, 317–326.
- Pike W., Staufner U., Hecht M., Goetz W., Parrat D., Sykulskaw-Lawrence H., Vijendran S. and Madsen M. B. (2011) Quantification of the dry history of the Martian soil inferred from in situ microscopy. *Geophys. Res. Lett.* **38**, L24201.
- Probyn T. A. (1987) Ammonium regeneration by microplankton in an upwelling environment. *Mar. Ecol. Prog. Ser.* **37**, 64.
- Qu J., Huang N., Dong G. and Zhang W. (2001) The role and significance of the Gobi Desert pavement in controlling sand movement on the cliff top near the Dunhuang Magao Grottoes. *J. Arid Environ.* **48**, 357–371.
- Quade J., Chivas A. and McCulloch M. (1995) Strontium and carbon isotope tracers and the origins of soil carbonate in South Australia and Victoria. *Palaeogeogr. Palaeoclimatol. Palaeoecol.* **113**, 103–117.
- Quinn P. K., Charlson R. J. and Bates T. S. (1988) Simultaneous observations of ammonia in the atmosphere and ocean. *Nature* **335**, 336–338.
- Quinn P. K., Bates T. S., Johnson J. E., Covert D. S. and Charlson R. J. (1990) Interactions between the sulfur and reduced nitrogen cycles over the central Pacific Ocean. *J. Geophys. Res.* **95**, 16405–16416.
- Quinn P., Barrett K., Dentener F., Lipschultz F. and Six K. (1996) Estimation of the air/sea exchange of ammonia for the North Atlantic Basin. *Biogeochemistry* **35**, 275–304.
- Quinn R., Zent A., Grunthaner F., Ehrenfreund P., Taylor C. and Garry J. (2005) Detection and characterization of oxidizing acids in the Atacama Desert using the Mars Oxidation Instrument. *Planet. Space Sci.* **53**, 1376–1388.
- Rech J. A., Quade J. and Hart W. S. (2003) Isotopic evidence for the source of Ca and S in soil gypsum, anhydrite and calcite in

- the Atacama Desert, Chile. *Geochim. Cosmochim. Acta* **67**, 575–586.
- Reheis M. C. and Kihl R. (1995) Dust deposition in southern Nevada and California, 1984–1989: relations to climate, source area, and source lithology. *J. Geophys. Res.* **100**, 8893–8918.
- Renard J. J., Calidonna S. E. and Henley M. V. (2004) Fate of ammonia in the atmosphere—a review for applicability to hazardous releases. *J. Hazard. Mater.* **108**, 29–60.
- Riha K.M., The use of stable isotopes to constrain the nitrogen cycle, PhD dissertation, Purdue University, 2013.
- Rutllant J., Muñoz R. and Garreaud R. (2013) Meteorological observations on the northern Chilean coast during VOCALS-REx. *Atmos. Chem. Phys.* **13**, 3409–3422.
- Ryerson T., Buhr M., Frost G., Goldan P., Holloway J., Hübler G., Jobson B., Kuster W., McKeen S. and Parrish D. (1998) Emissions lifetimes and ozone formation in power plant plumes. *J. Geophys. Res.* **103**, 22569–22583.
- Saavedra-Pellitero M., Flores J. A., Baumann K. H. and Sierro F. J. (2010) Coccolith distribution patterns in surface sediments of Equatorial and Southeastern Pacific Ocean. *Geobios* **43**, 131–149.
- Schemenauer R. S. and Cereceda P. (1992) The quality of fog water collected for domestic and agricultural use in Chile. *J. Appl. Meteorol.* **31**, 275–290.
- Schemenauer R. S. and Cereceda P. (1994) A proposed standard fog collector for use in high-elevation regions. *J. Appl. Meteorol.* **33**, 1313–1322.
- Schemenauer R. S. and Isaac G. (1984) The Importance of cloud top lifetime in the description of natural cloud characteristics. *J. Appl. Meteorol.* **23**, 267–279.
- Schemenauer R. S. and Joe P. I. (1989) The collection efficiency of a massive fog collector. *Atmos. Res.* **24**, 53–69.
- Schemenauer R. S., Fuenzalida H. and Cereceda P. (1988) A neglected water resource: the Camanchaca of South America. *Bull. Am. Meteorol. Soc.* **69**, 138–147.
- Seinfeld J. H. and Pandis S. N. (2006) *Atmospheric Chemistry and Physics: From air Pollution to Climate Change*. John Wiley & Sons, New York.
- Servicio Nacional de Geología y Minería (SERNAGEOMIN) (2003) Mapa Geológico de Chile: versión digital. Servicio Nacional de Geología y Minería, Publicación Geológica Digital, No. 4 (CD-ROM, versión 1.0, 2003), Santiago (in Spanish).
- Shaw G. E. (1991) Aerosol chemical components in Alaska air masses: 2. Sea salt and marine product. *J. Geophys. Res.* **96**, 22369–22372.
- Sievering H., Ennis G., Gorman E. and Nagamoto C. (1990) Size distributions and statistical analysis of nitrate, excess sulfate, and chloride deficit in the marine boundary layer during GCE/CASE/WATOX. *Global Biogeochem. Cycles* **4**, 395–405.
- Sievering H., Cainey J., Harvey M., McGregor J., Nichol S. and Quinn P. (2004) Aerosol non-sea-salt sulfate in the remote marine boundary layer under clear-sky and normal cloudiness conditions: ocean-derived biogenic alkalinity enhances sea-salt sulfate production by ozone oxidation. *J. Geophys. Res.* **109**, D19317.
- Slinn W., Radke L. and Katen P. (1982) Inland transport, mixing and dry deposition of sea-salt particles. In *Precipitation Scavenging, Dry Deposition and Resuspension, vol. 1: Precipitation Scavenging* (eds. H. R. Pruppacher, R. G. Semonin and W. G. N. Slinn). Elsevier, Santa Monica, pp. 1037–1046.
- Song C. H. and Carmichael G. R. (2001) A three-dimensional modeling investigation of the evolution processes of dust and sea-salt particles in East Asia. *J. Geophys. Res.* **106**, 18131–18154.
- Stoertz G. E. and Erickson G. E. (1974) Geology of salars in northern Chile. *US Geol. Surv. Prof. Pap.*, 811.
- Stuut J. B. W., Kasten S., Lamy F. and Hebbeln D. (2007) Sources and modes of terrigenous sediment input to the Chilean continental slope. *Quatern. Int.* **161**, 67–76.
- Thiemens M. H. (1999) Mass-independent isotope effects in planetary atmospheres and the early solar system. *Science* **283**, 341.
- Thiemens M. H. (2006) History and applications of mass-independent isotope effects. *Annu. Rev. Earth Planet. Sci.* **34**, 217–262.
- Tsunogai S. (1971) Ammonia in the oceanic atmosphere and the cycle of nitrogen compounds through the atmosphere and the hydrosphere. *Geochem. J.* **5**, 57–67.
- Vogt R. (1996) A mechanism for halogen release from sea-salt. *Nature* **383**, 26.
- Warneck P. (2000) *Chemistry of the Natural Atmosphere*. Academic Press, San Diego, p. 927.
- Westbeld A., Klemm O., Griefbaum F., Sträter E., Larrain H., Osses P. and Cereceda P. (2009) Fog deposition to a Tillandsia carpet in the Atacama Desert. *Ann. Geophys.* **27**, 3571–3576.
- Whitney F. and Freeland H. (1999) Variability in upper-ocean water properties in the NE Pacific Ocean. *Deep Sea Res. II* **46**, 2351–2370.
- Wolfe S. A. and Nickling W. G. (1993) The protective role of sparse vegetation in wind erosion. *Prog. Phys. Geogr.* **17**, 50–68.
- Yamamoto N., Nishiura H., Honjo T., Ishikawa Y. and Suzuki K. (1995) A long-term study of atmospheric ammonia and particulate ammonium concentrations in Yokohama, Japan. *Atmos. Environ.* **29**, 97–103.
- Yang M., Huebert B., Blomquist B., Howell S., Shank L., McNaughton C., Clarke A., Hawkins L., Russell L. and Covert D. (2011) Atmospheric sulfur cycling in the southeastern Pacific – longitudinal distribution, vertical profile, and diel variability observed during VOCALS-Rex. *Atmos. Chem. Phys.* **11**, 5079–5097.
- Zhuang H., Chan C. K., Fang M. and Wexler A. S. (1999) Formation of nitrate and non-sea-salt sulfate on coarse particles. *Atmos. Environ.* **33**, 4223–4233.
- Ziereis H. and Arnold F. (1986) Gaseous ammonia and ammonium ions in the free troposphere. *Nature* **321**, 503–505.

Associate editor: Anthony Dosseto